Supporting information for

Denticity Governs on the Formation of β-Thioketiminato Tri-Copper(I) and Mono-Copper(I) Complexes

Venkata Sai Sashankh Penki[a], Yu-Lun Chang[a], Hsing-Yin Chen[a], Yu-Ting Chu[a,b], Yu-Ting Kuo[a,b], Dorothy Priyanka Dorairaj[a,c], Sri Sudewi[a,d], Shang-Wu Ding[b], and Sodio C.N. Hsu[a,b,e]*

[a] *Department of Medicinal and Applied Chemistry, Kaohsiung Medical University, Kaohsiung 80708, Taiwan.*
[b]*Department of Chemistry, National Sun Yat-Sen University, Kaohsiung 80424, Taiwan.*
[c]*Department of Chemistry, National Institute of Technology, Tiruchirappalli 620015, India*
[d]*Department of pharmacy, Faculty of Mathematic and Natural science, Universitas Sam Ratulangi, Manado 95115, Indonesia.*
[e]*Department of Medical Research, Kaohsiung Medical University Hospital, Kaohsiung 80708, Taiwan.*

Table of contents

Ligand Synthesis:

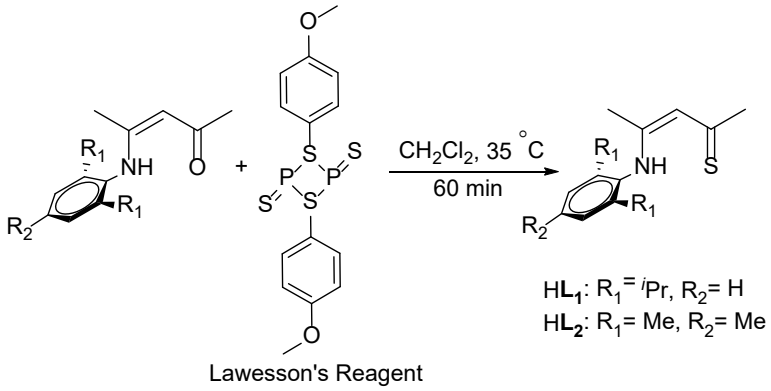

HL1. The reaction of (Z)-4-((2,6-diisopropylphenyl)amino)pent-3-en-2-one (5.00 g, 19.27 mmol), and Lawesson's reagent (3.89 g, 9.637 mmol) were dissolved in dichloromethane (50ml) and heated at 35 °C for 1h. The volatiles were removed under vacuum to give a reddish orange oil that was purified by column chromatography ethyl acetate/hexane 1:10 ratio. Solvent is removed by vacuum to give reddish-orange oil. Recrystallization of the crude product from hexane gave pure H**L1** as reddish-orange crystals (4.45 g, 85 % yield). (C_6D_6, 400 MHz, 298K, δ): 15.85 (bs, 1H, NH), 7.12 (m, 1H, Ar-H), 7.00 (d, 2H, Ar-H), 6.10 (s, 1H, backbone-CH), 2.95 (septet, J = 6.8 Hz, 2H, C*H*$(CH_3)_2$), 2.67 (s, 3H, backbone-C*H*$_3$), 1.38(s, 3H, backbone-C*H*$_3$), 1.03 (dd, J = 4.0 Hz, 12H, CH(C*H*$_3)_2$). $^{13}C\{^1H\}$ NMR (C_6D_6, 100 MHz, 298K, δ): 209.10, 165.28, 145.62, 133.13, 128.98, 124.00,112.45, 39.15, 29.02, 25.09, 22.48, 20.39. Anal. Calcd for $C_{17}H_{25}NS$: C, 74,13; H, 9.15; N, 5.09. Found: C, 74.15; H, 9.11; N, 5.08.

HL2. The reaction of (Z)-4-(mesitylamino)pent-3-en-2-one (5 g, 23.0 mmol) and Lawesson's reagent (4.64 g, 11.50 mmol) in dichloromethane gave purified by column chromatography ethyl acetate/hexane 1:10 ratio. Solvent is removed by vacuum to give reddish-orange oil. Recrystallization of the crude product from hexane gave pure H**L2** as reddish-orange crystals (4.66 g, 87 % yield). ^1H NMR (C_6D_6, 400 MHz, 298K, δ): 15.57 (bs, 1H, NH), 6.02 (s, 2H, Ar-H), 6.09 (s, 1H, backbone-CH), 2.67 (s, 3H, backbone-C*H*$_3$), 2.06 (s, 3H, *para* ArC*H*$_3$), 1.93 (s, 6H, *ortho* ArCH_3), 1.34 (s, 3H, backbone-C*H*$_3$). $^{13}C\{^1H\}$ NMR (C_6D_6, 100 MHz, 298K, δ): 208.70, 165.72, 137.44, 134.71, 133.51, 129.38, 112.64, 39.16, 20.95, 20.03, 18.13. Anal. % Calcd for $C_{14}H_{19}NS$: C, 72,05; H, 8.21; N, 6.00. Found: C, 72.10; H, 8.11; N, 5.96.

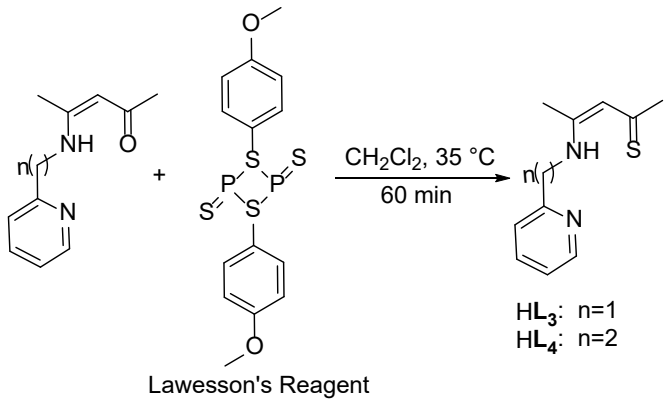

***HL3*:** The reaction of (Z)-4-((pyridin-2-ylmethyl)amino)pent-3-en-2-one (5.00 g, 26.28 mmol), and Lawesson's reagent (5.30 g, 13.14 mmol) were dissolved in dichloromethane (50ml) and heated at 35 °C for 1h. The volatiles were removed under vacuum to give a reddish-brown oil was purified by column chromatography ethyl acetate/ dichloromethane 1:10 ratio. Solvent is removed by vacuum to give reddish orange oil. Recrystallization of the crude product from dichloromethane gave pure H**L3** as reddish-brown crystals (3.48 g, 73.4 % yield). ^{1}H NMR (C_6D_6, 400 MHz, 298K, δ): 14.65 (bs, 1H, NH), 8.32 (d, 1H, *J* =4 Hz, Py1), 7.03 (ddd, 1H, *J* = 7.6 Hz, Py2), 6.95 (d, *J* = 8 Hz, 1H, Py4), 6.62 (m, 1H, Py3), 5.92 (s, 1H, backbone C*H*), 4.16 (s, 2H, CH_2Py), 2.61 (s, 3H, backbone-CH_3), 1.46 (s, 3H, backbone-CH_3). ^{13}C{^{1}H} NMR (C_6D_6, 100 MHz, 298K, δ): 207.06, 165.66, 156.79, 149.70, 136.81, 122.50, 121.22, 113.24, 48.97, 39.16, 20.22. Anal. % Calcd for $C_{11}H_{14}N_2S$: C, 64,04; H, 6.84; N, 13.58. Found: C, 64.05; H, 6.82; N, 13.55.

***HL4*.** The reaction of (Z)-4-((2-(pyridin-2-yl)ethyl)amino)pent-3-en-2-one (5 g, 24.50 mmol) and Lawesson's reagent (4.95 g, 11.50 mmol) in dichloromethane gave purified by column chromatography ethyl acetate/ dichloromethane 1:10 ratio. Solvent is removed by vacuum to give reddish-orange oil. Recrystallization of the crude product from hexane gave pure H**L4** as reddish-brown crystals (4.20 g, 77.80 % yield). ^{1}H NMR (C_6D_6, 400 MHz, 298K, δ): 14.32 (bs, 1H, NH), 8.39 (d, 1H, *J* =4 Hz, Py1), 7.05 (ddd, 1H, *J* = 7.6 Hz, Py2), 6.79 (d, *J* = 8 Hz, 1H, Py4), 6.63 (dd, 1H, Py3), 5.80 (s, 1H, backbone C*H*), 3.32 (q, 2H, CH_2CH_2Py), 2.72 (t, 2H, CH$_2$CH_2Py), 2.58 (s, 3H, backbone-CH_3), 1.33 (s, 3H, backbone-CH_3). ^{13}C{^{1}H} NMR (C_6D_6, 100 MHz, 298K, δ): 205.01, 165.20, 158.12, 149.72, 136.28, 123.95, 121.82, 112.72, 43.08, 38.95, 37.85, 19.84. Anal. % Calcd for $C_{12}H_{16}N_2S$: C, 65,42; H, 7.32; N, 12.71. Found: C, 65.39; H, 7.32; N, 12.74.

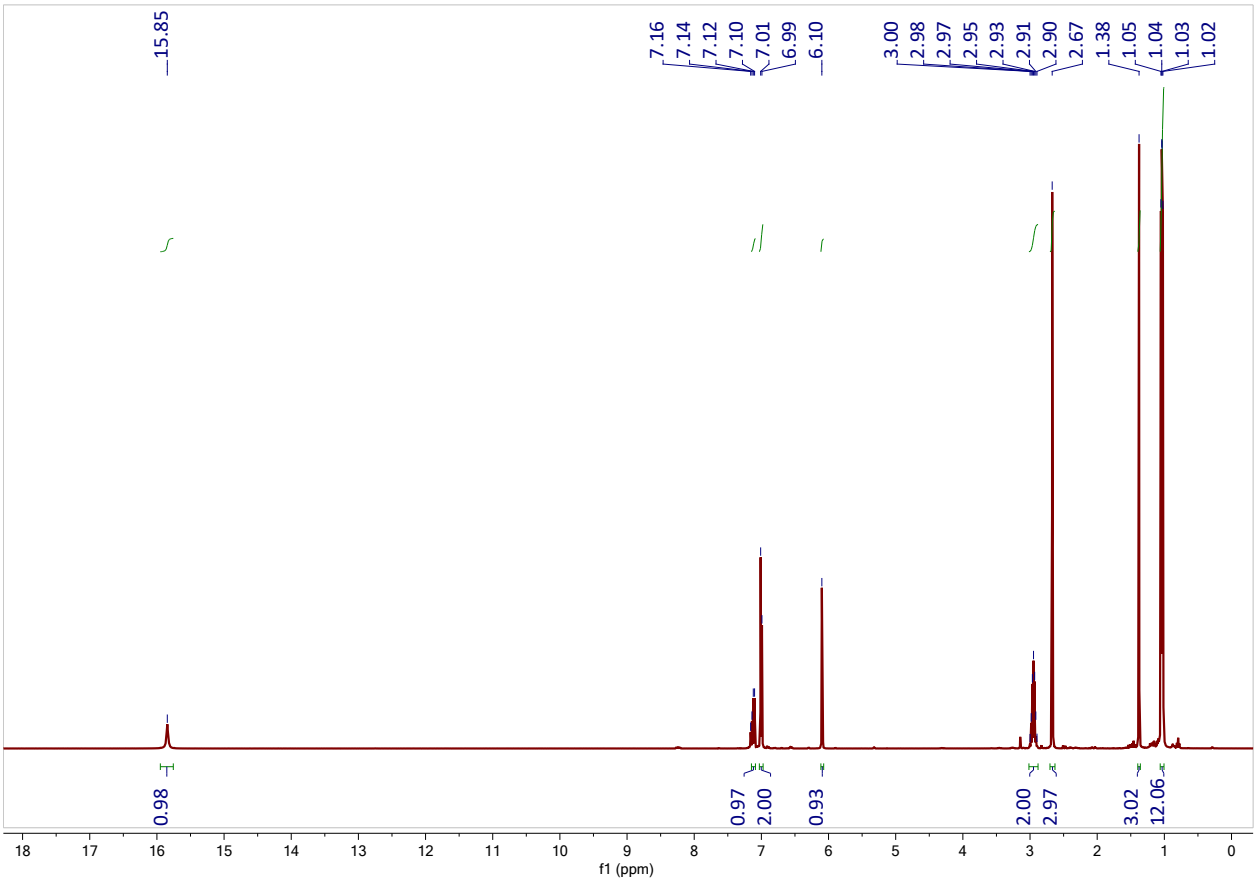

Figure S1. ^{1}H NMR spectrum of H**L**$_1$ in C_6D_6 (400 MHz, 298 K).

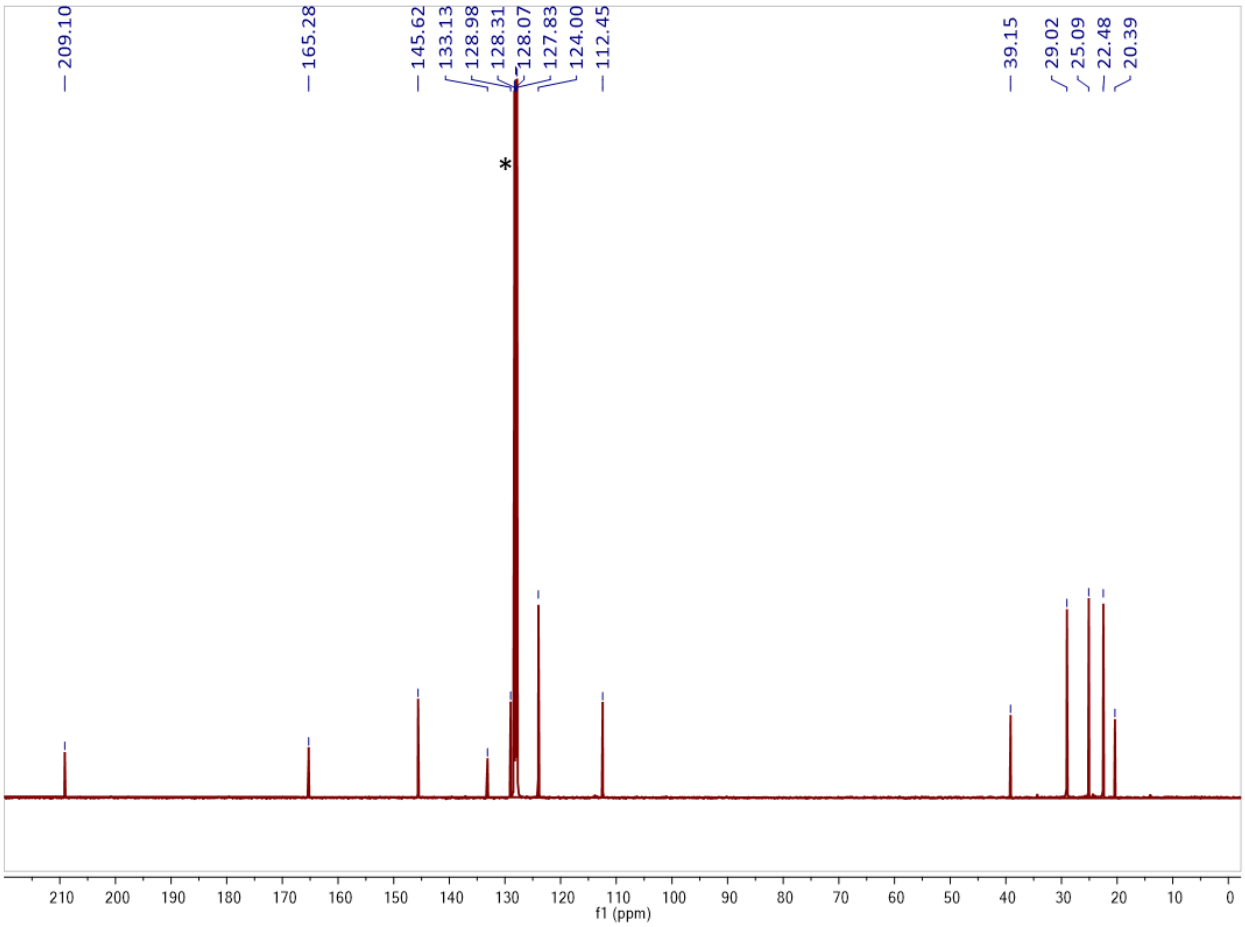

Figure S2. ^{13}C NMR spectrum of H**L**$_1$ in C_6D_6 (100 MHz, 298 K). Solvent residual peaks are marked with an asterisk (*).

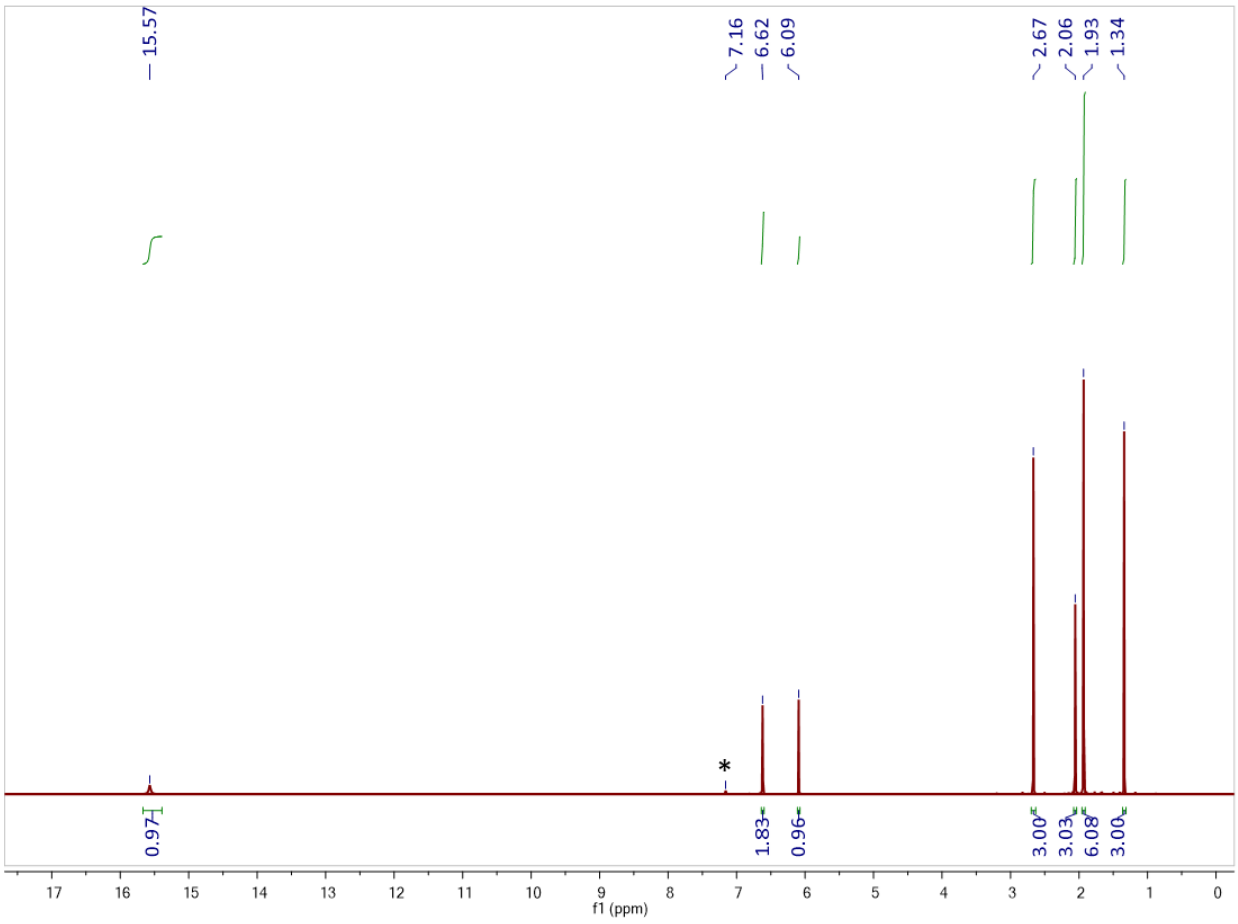

Figure S3. ^{1}H NMR spectrum of H**L₂** in C_6D_6 (400 MHz, 298 K). Solvent residual peaks are marked with an asterisk (*).

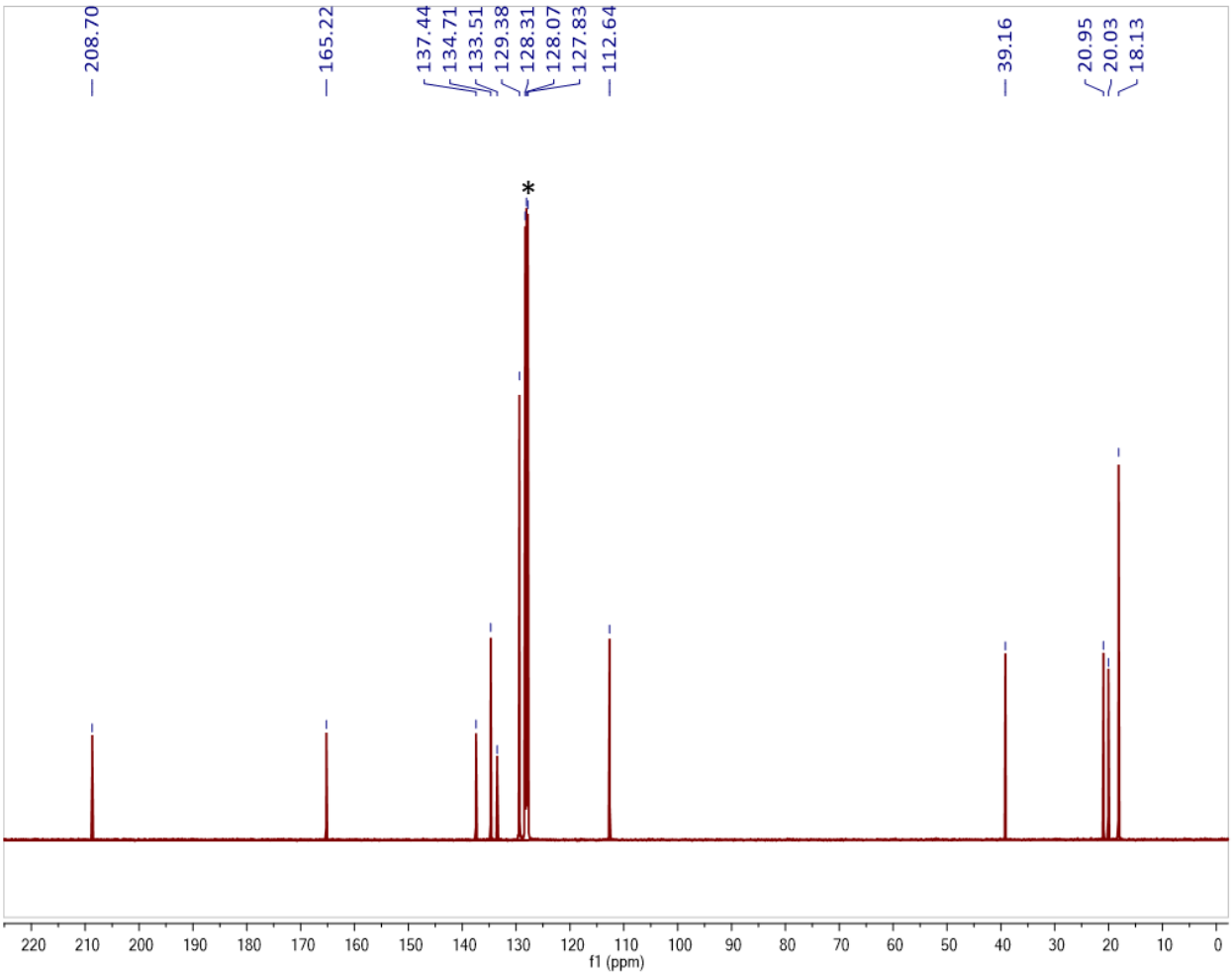

Figure S4. ^{13}C NMR spectrum of H**L**$_2$ in C_6D_6 (100 MHz, 298 K). Solvent residual peaks are marked with an asterisk (*).

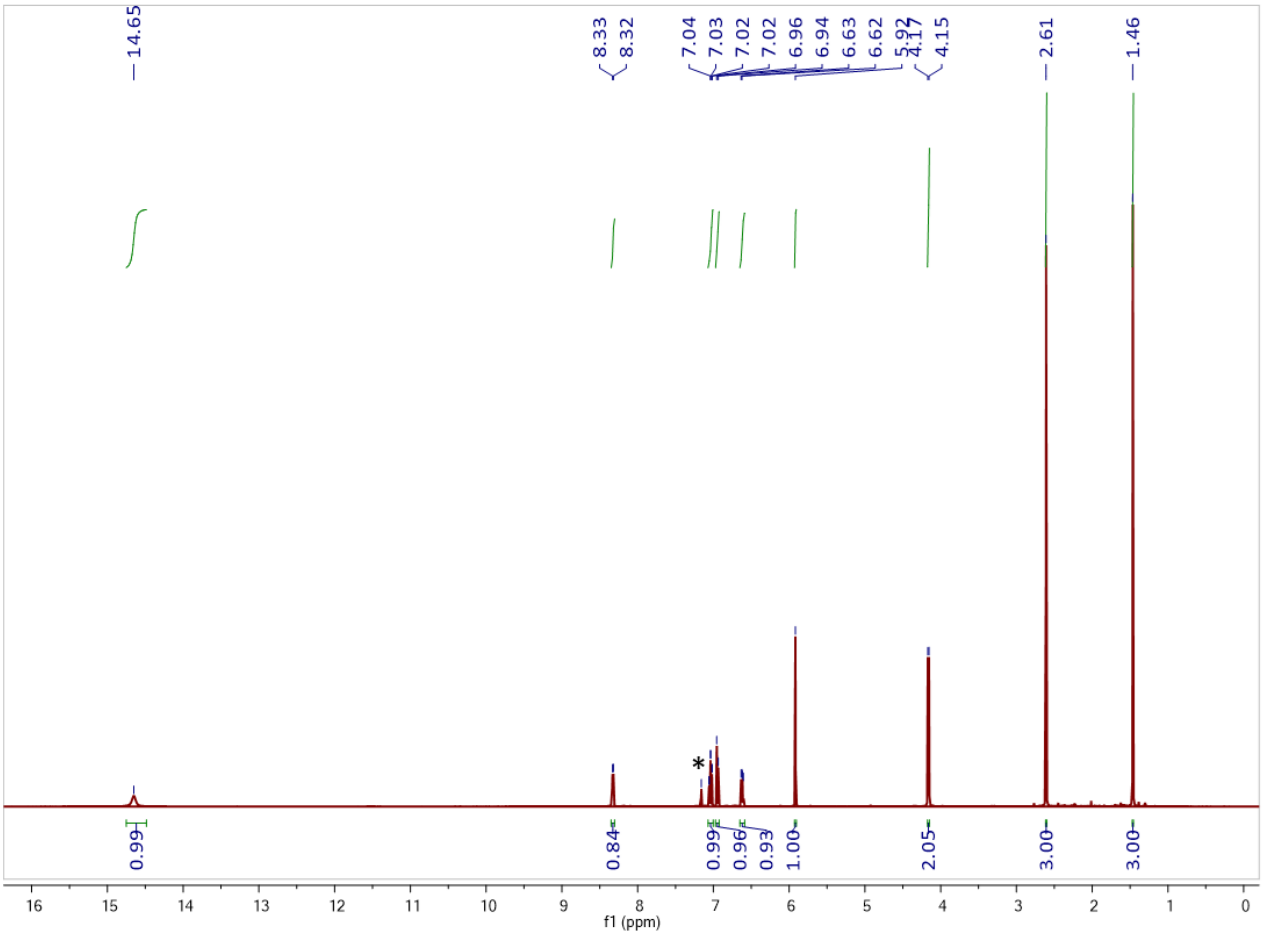

Figure S5. ^{1}H NMR spectrum of H**L*3*** in C_6D_6 (400 MHz, 298 K). Solvent residual peaks are marked with an asterisk (*).

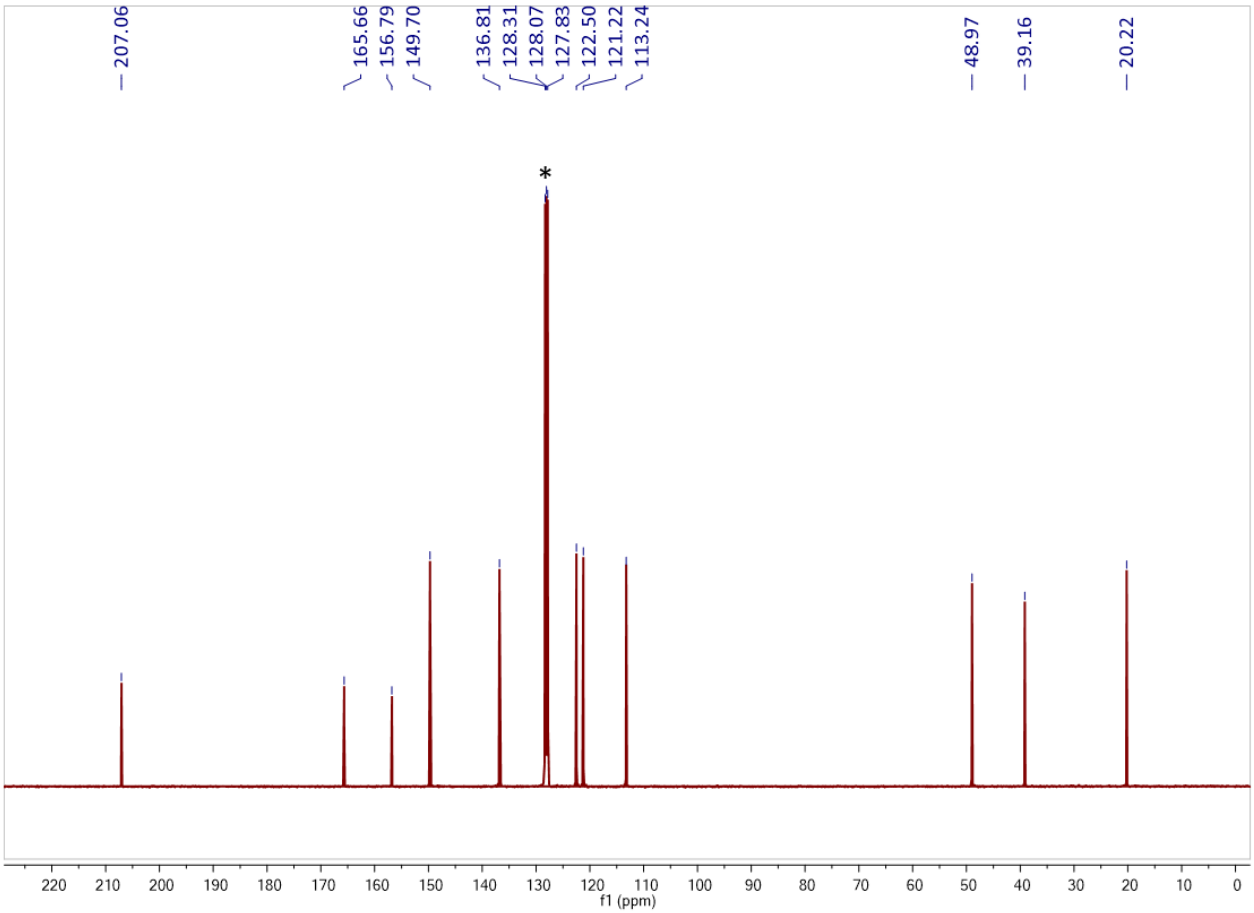

Figure S6. ^{13}C NMR spectrum of **HL3** in C_6D_6 (100 MHz, 298 K). Solvent residual peaks are marked with an asterisk (*).

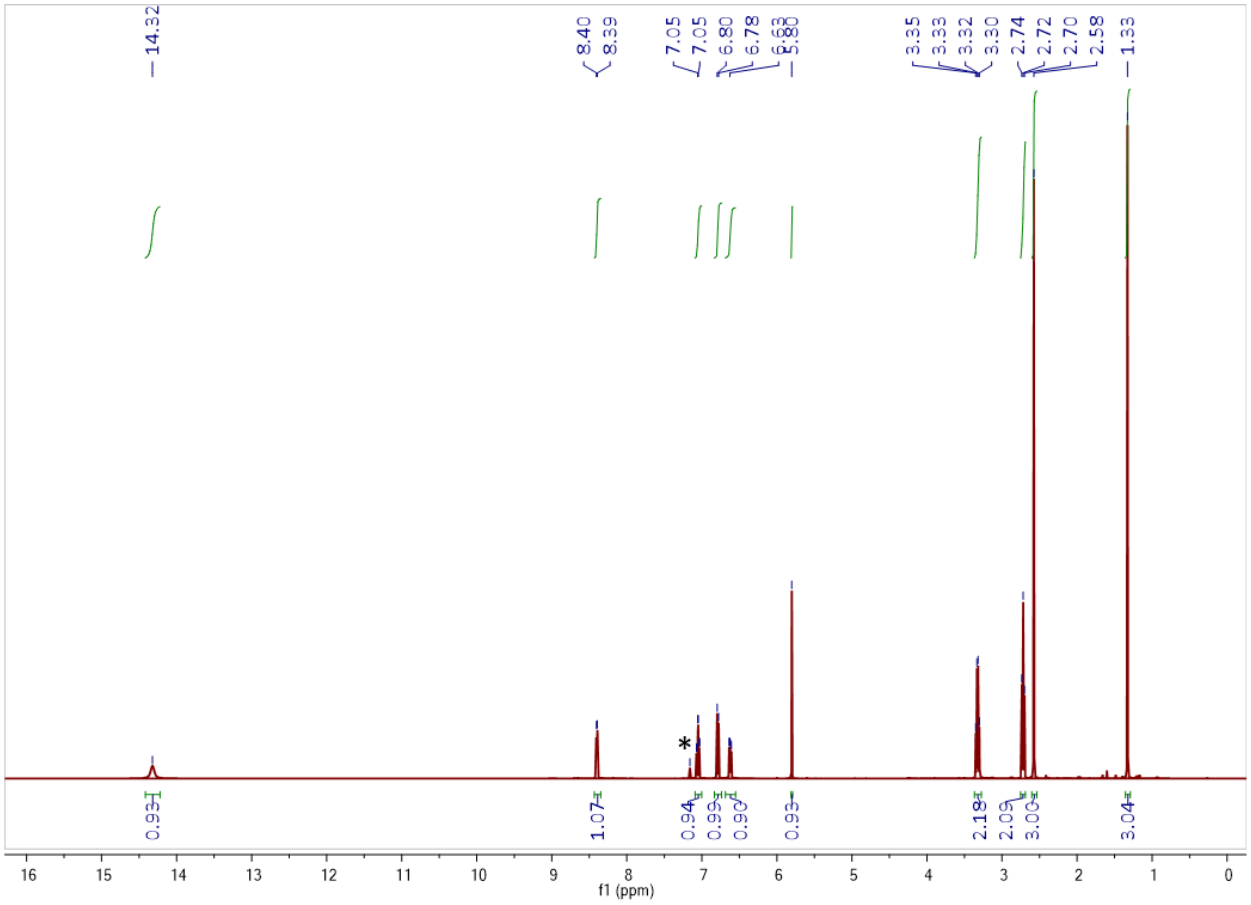

Figure S7. ^{1}H NMR spectrum of H**L**$_4$ in C_6D_6 (400 MHz, 298 K). Solvent residual peaks are marked with an asterisk (*).

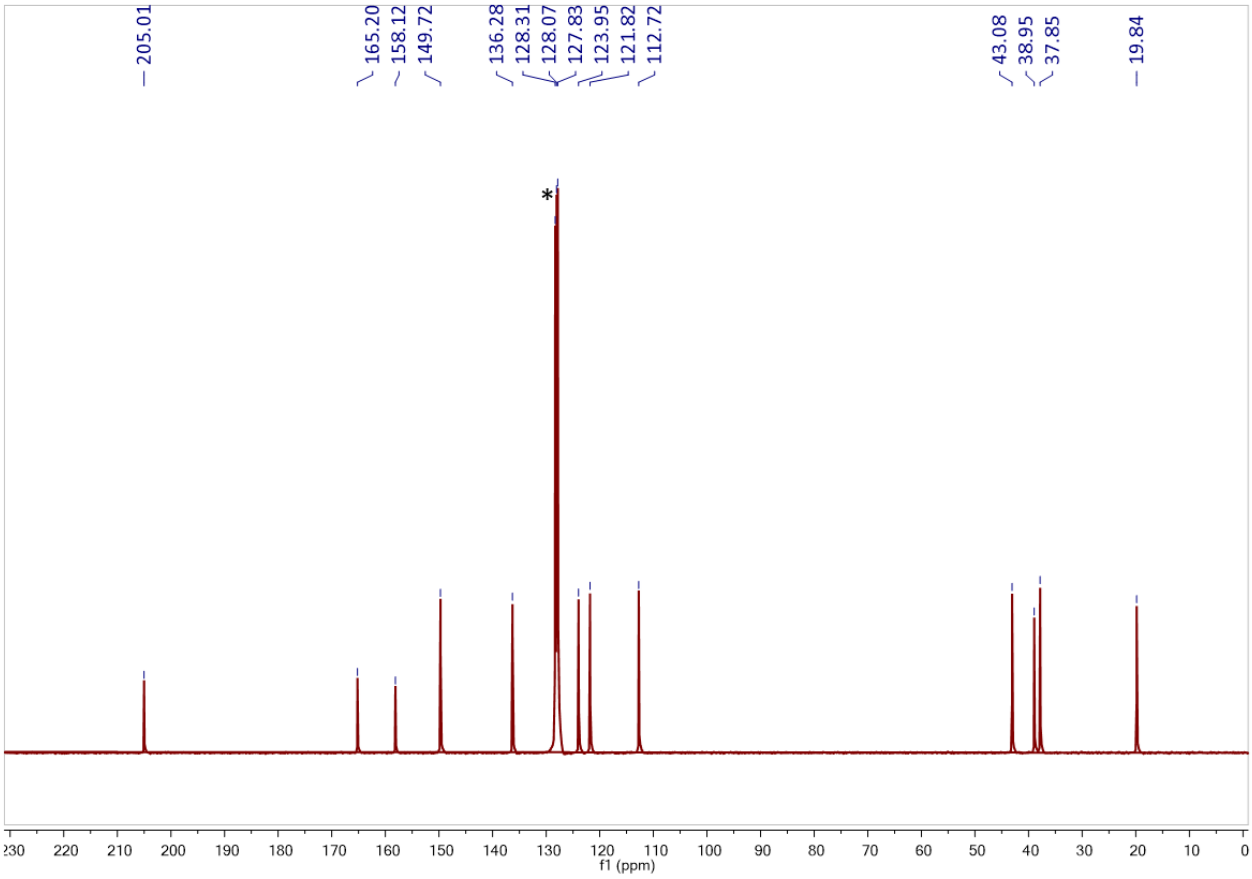

Figure S8. ^{13}C NMR spectrum of H**L4** in C_6D_6 (100 MHz, 298 K). Solvent residual peaks are marked with an asterisk (*).

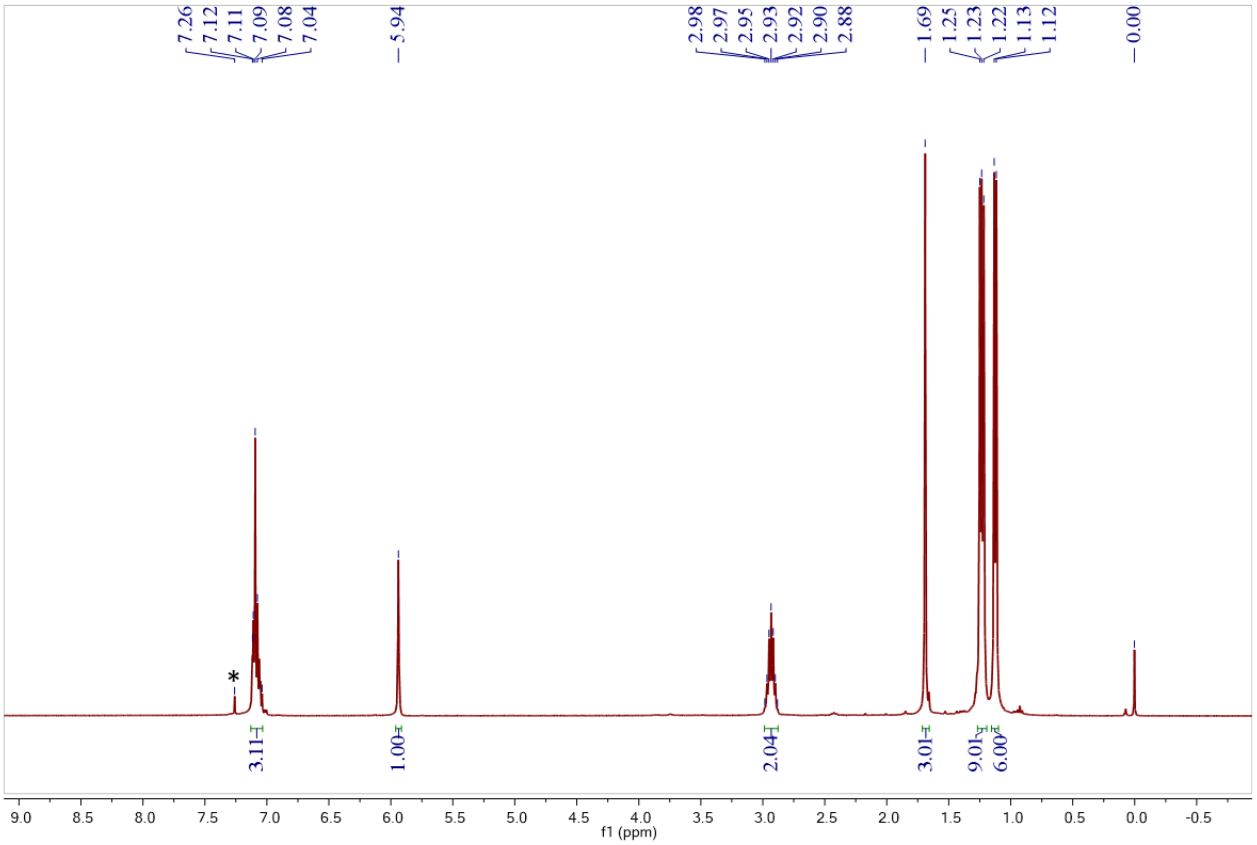

Figure S9. ^{1}H NMR spectrum of [**L**$_{1}$Cu]$_{3}$ in $CDCl_3$ (400 MHz, 298 K). Solvent residual peaks are marked with an asterisk (*).

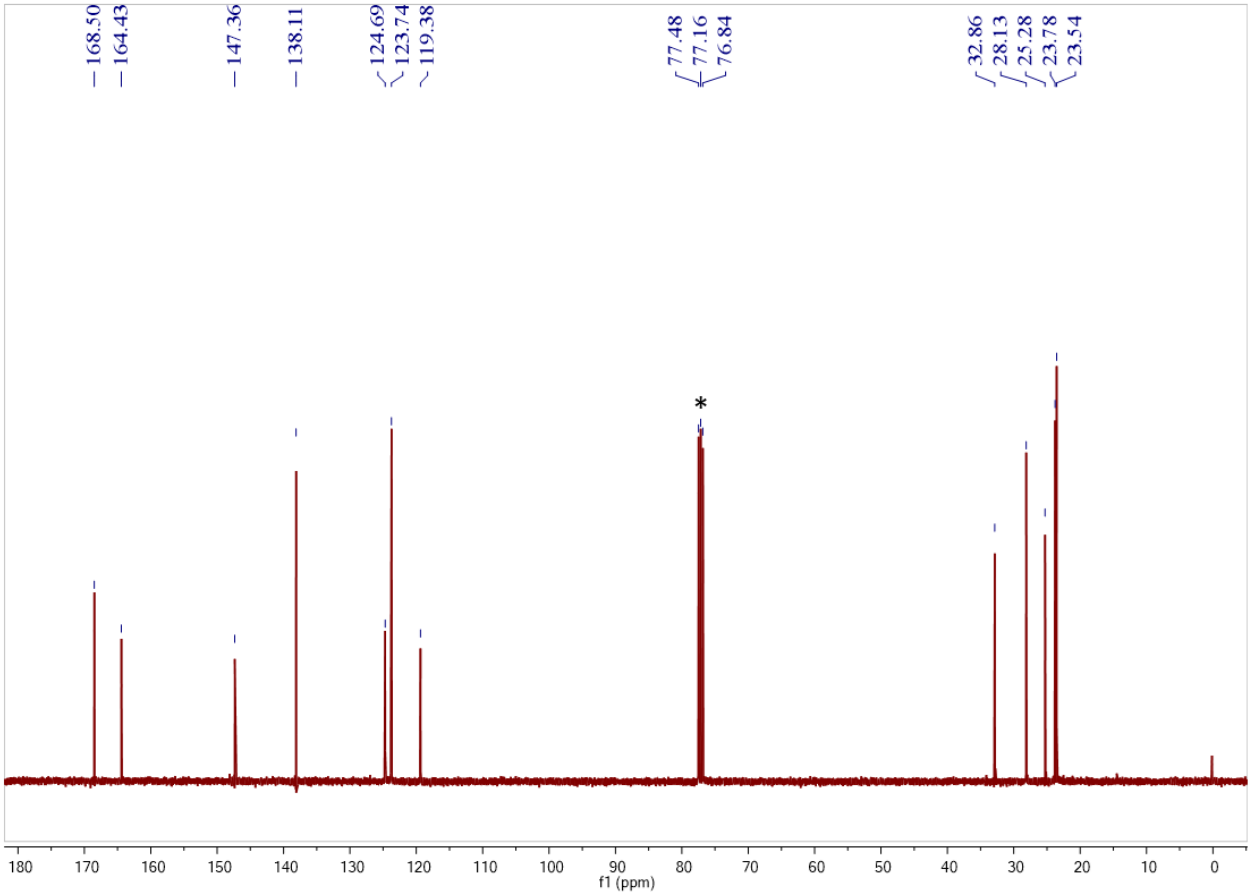

Figure S10. ^{13}C NMR spectrum of $[\mathbf{L_1}Cu]_3$ in $CDCl_3$ (100 MHz, 298 K). Solvent residual peaks are marked with an asterisk (*).

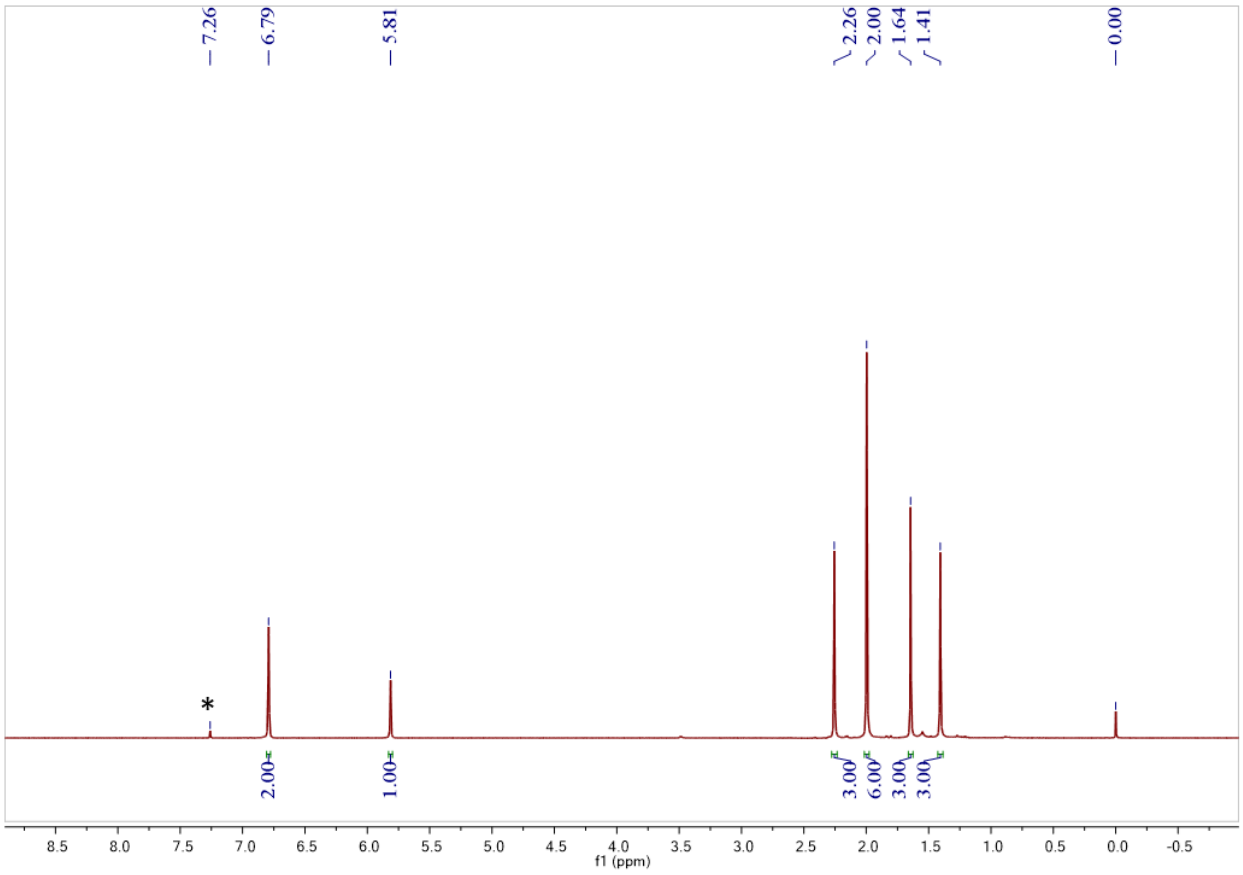

Figure S11. ^{1}H NMR spectrum of [**L**$_2$Cu]$_3$ in $CDCl_3$ (400 MHz, 298 K). Solvent residual peaks are marked with an asterisk (*).

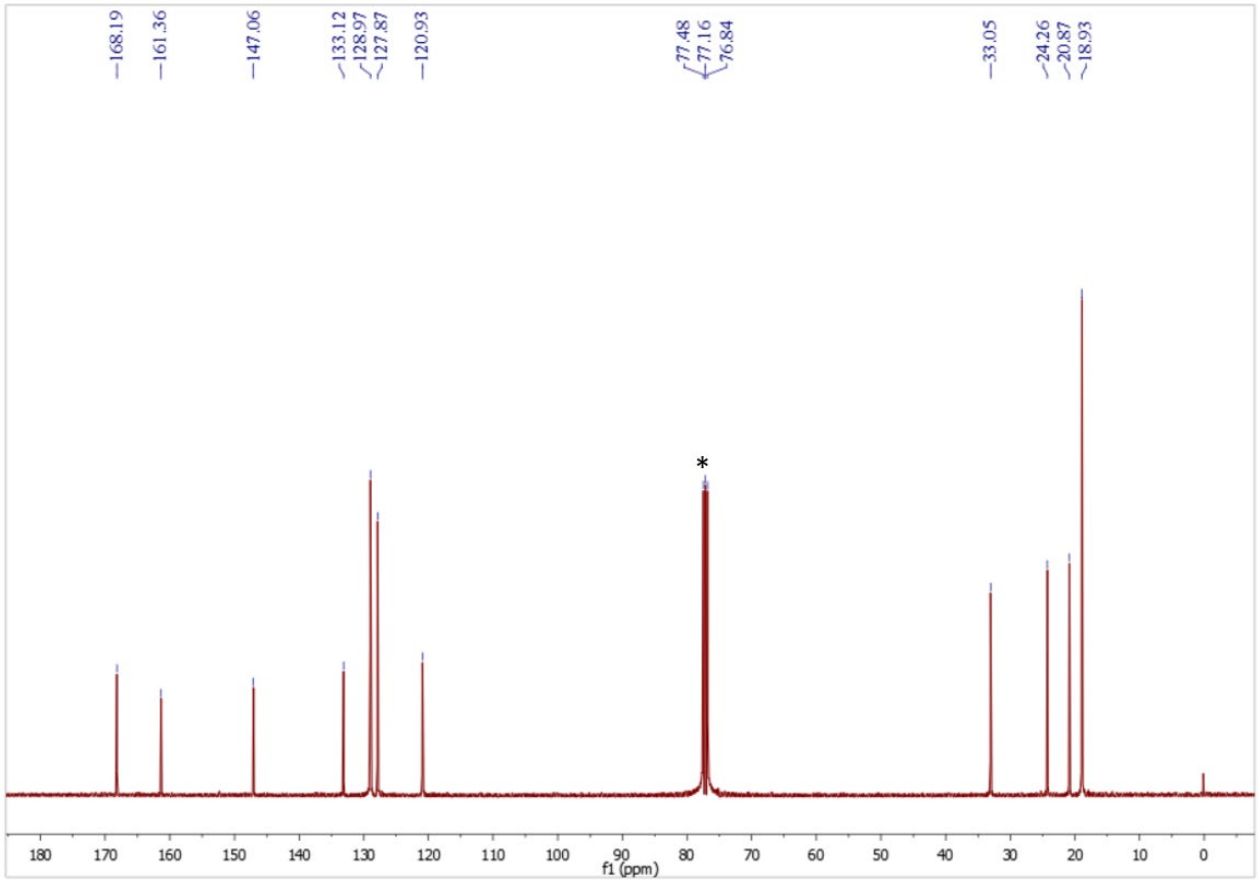

Figure S12. ^{13}C NMR spectrum of $[\mathbf{L_2}Cu]_3$ in $CDCl_3$ (100 MHz, 298 K). Solvent residual peaks are marked with an asterisk (*).

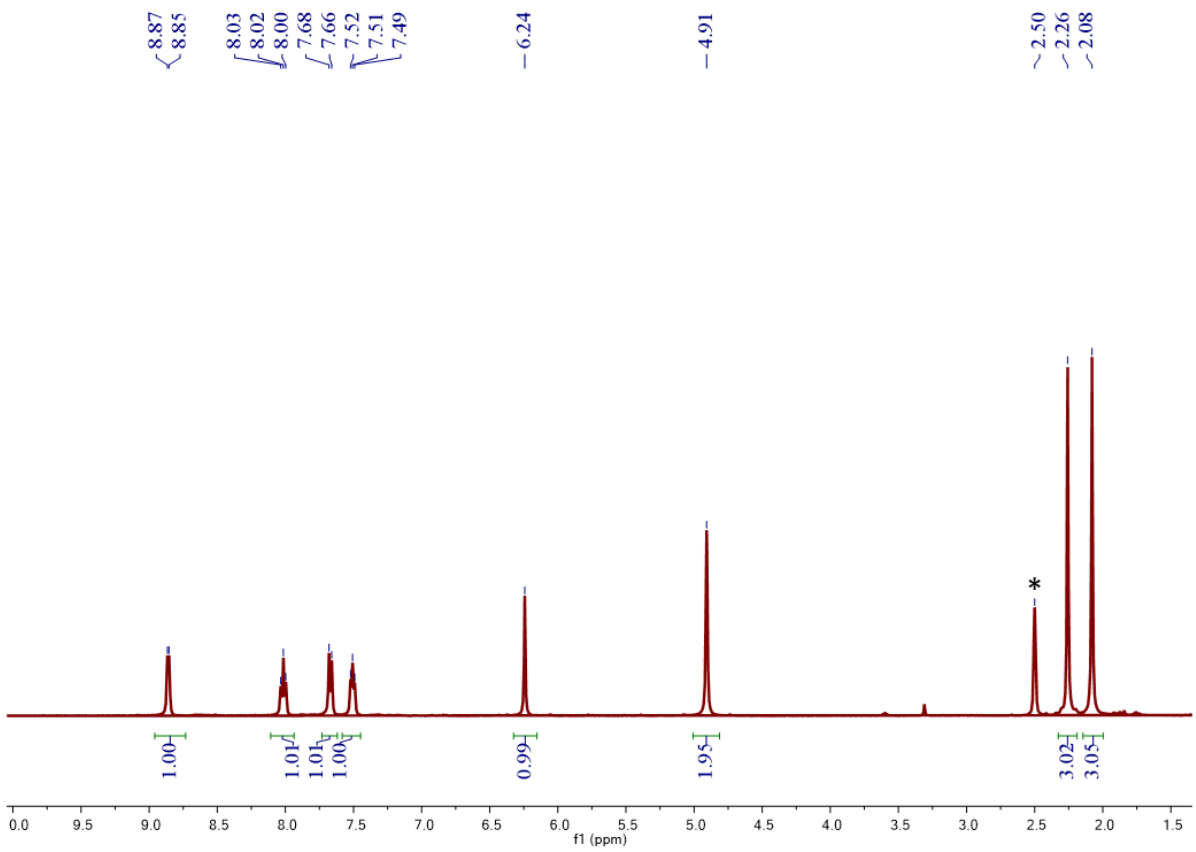

Figure S13. ^{1}H NMR spectrum of **L$_3$**Cu in DMSO-D$_6$ (400 MHz, 298 K). Solvent residual peaks are marked with an asterisk (*).

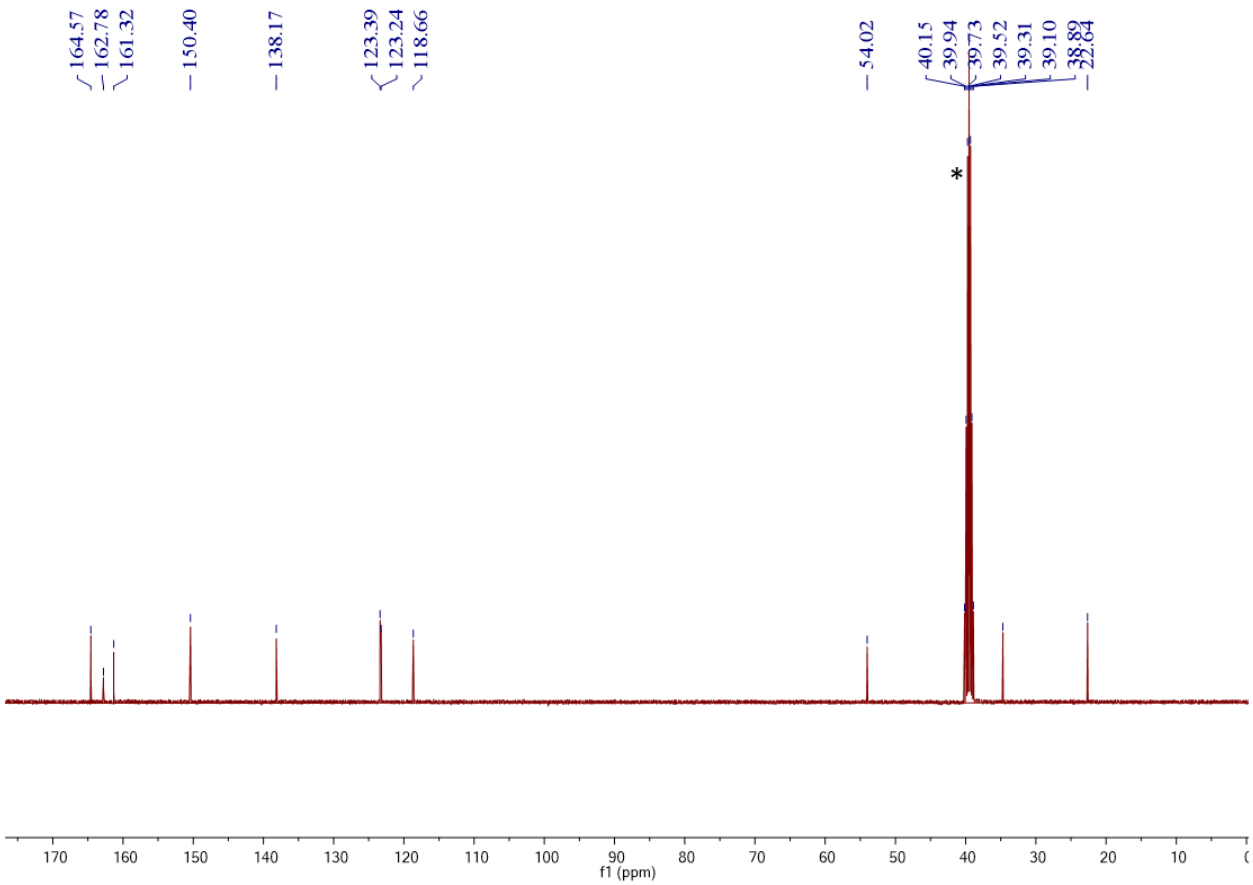

Figure S14. ^{13}C NMR spectrum of **L**$_3$Cu in DMSO-D_6 (100 MHz, 298 K). Solvent residual peaks are marked with an asterisk (*).

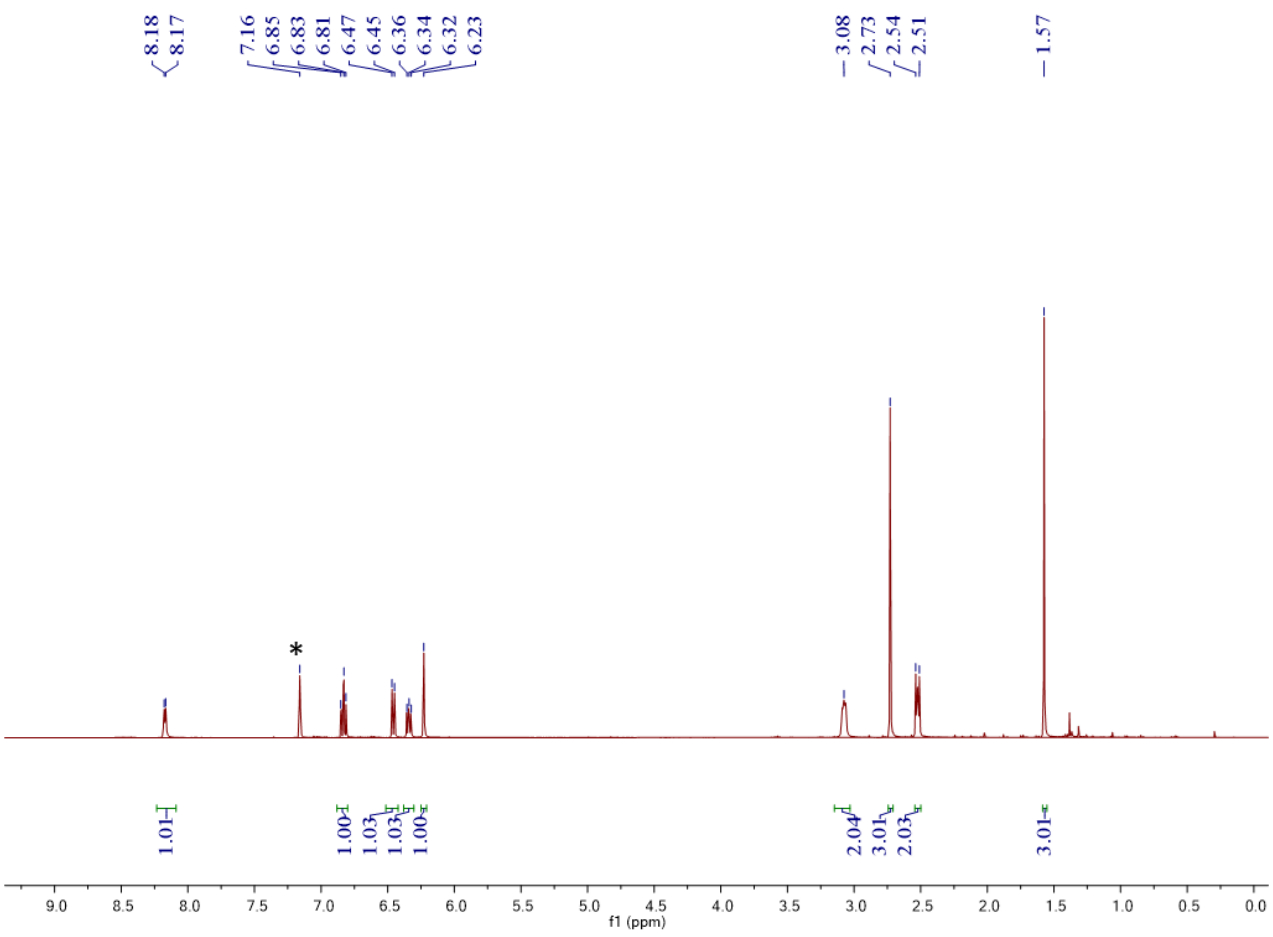

Figure S15. ^{1}H NMR spectrum of **L$_4$**Cu in C_6D_6 (400 MHz, 298 K). Solvent residual peaks are marked with an asterisk (*).

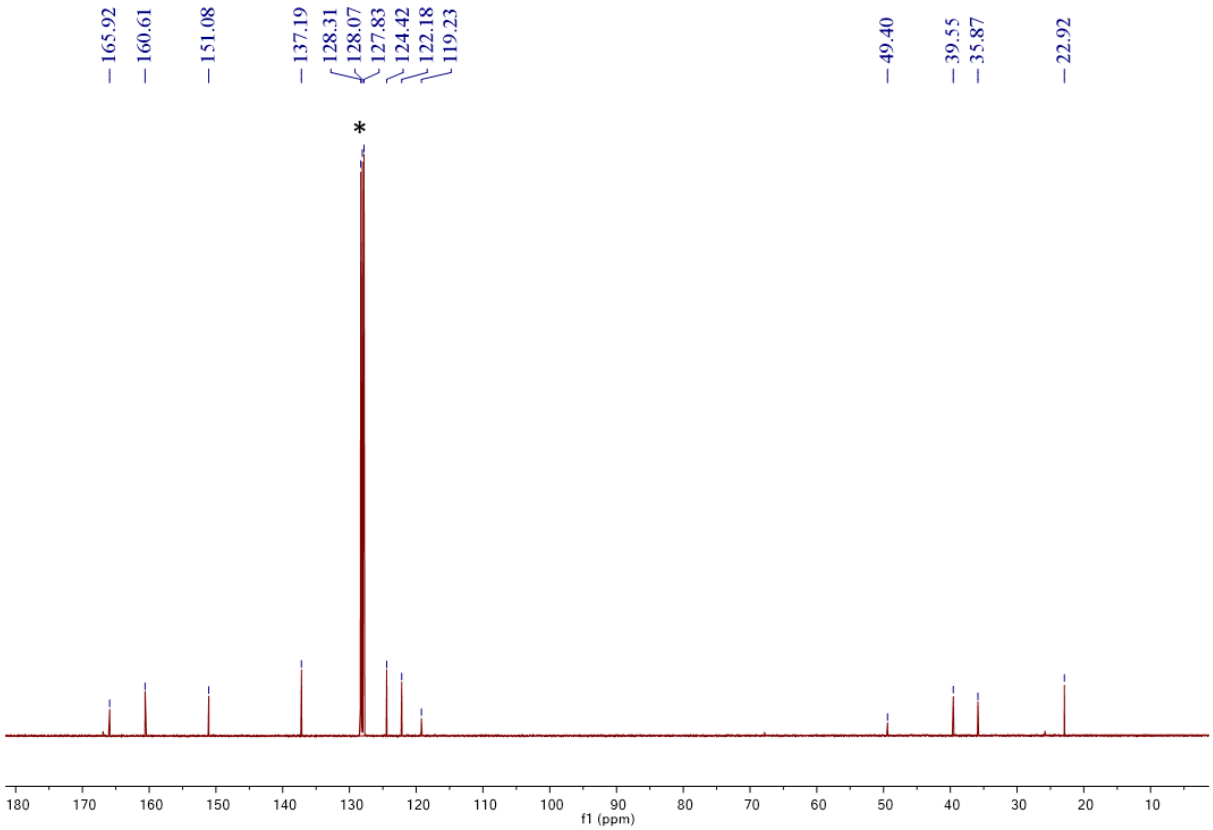

Figure S16. ^{13}C NMR spectrum of **L**$_4$Cu in C_6D_6 (100 MHz, 298 K). Solvent residual peaks are marked with an asterisk (*).

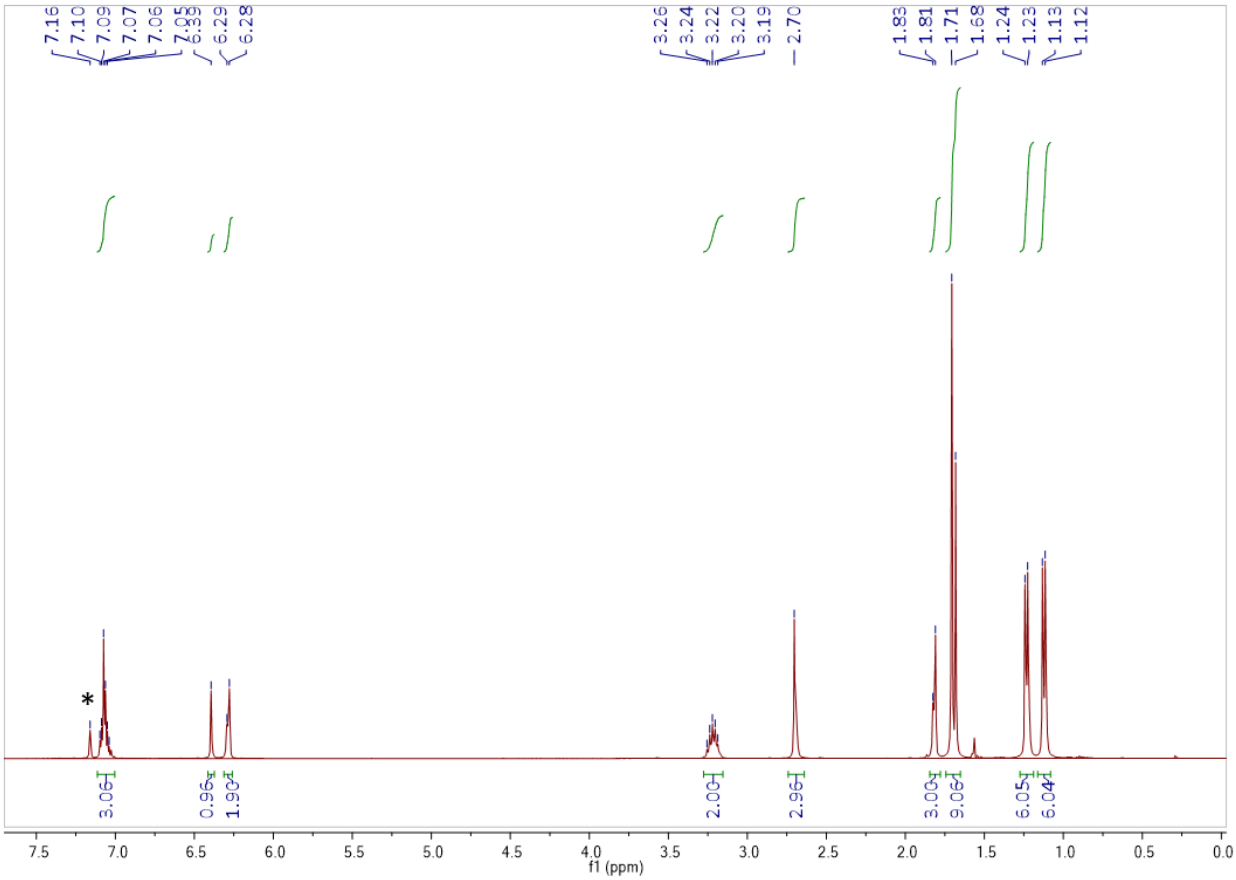

Figure S17. ^{1}H NMR spectrum of **L**$_{1}$Cu(2,4,6-CNC$_6$H$_2$Me$_3$) in C$_6$D$_6$ (400 MHz, 298 K). Solvent residual peaks are marked with an asterisk (*).

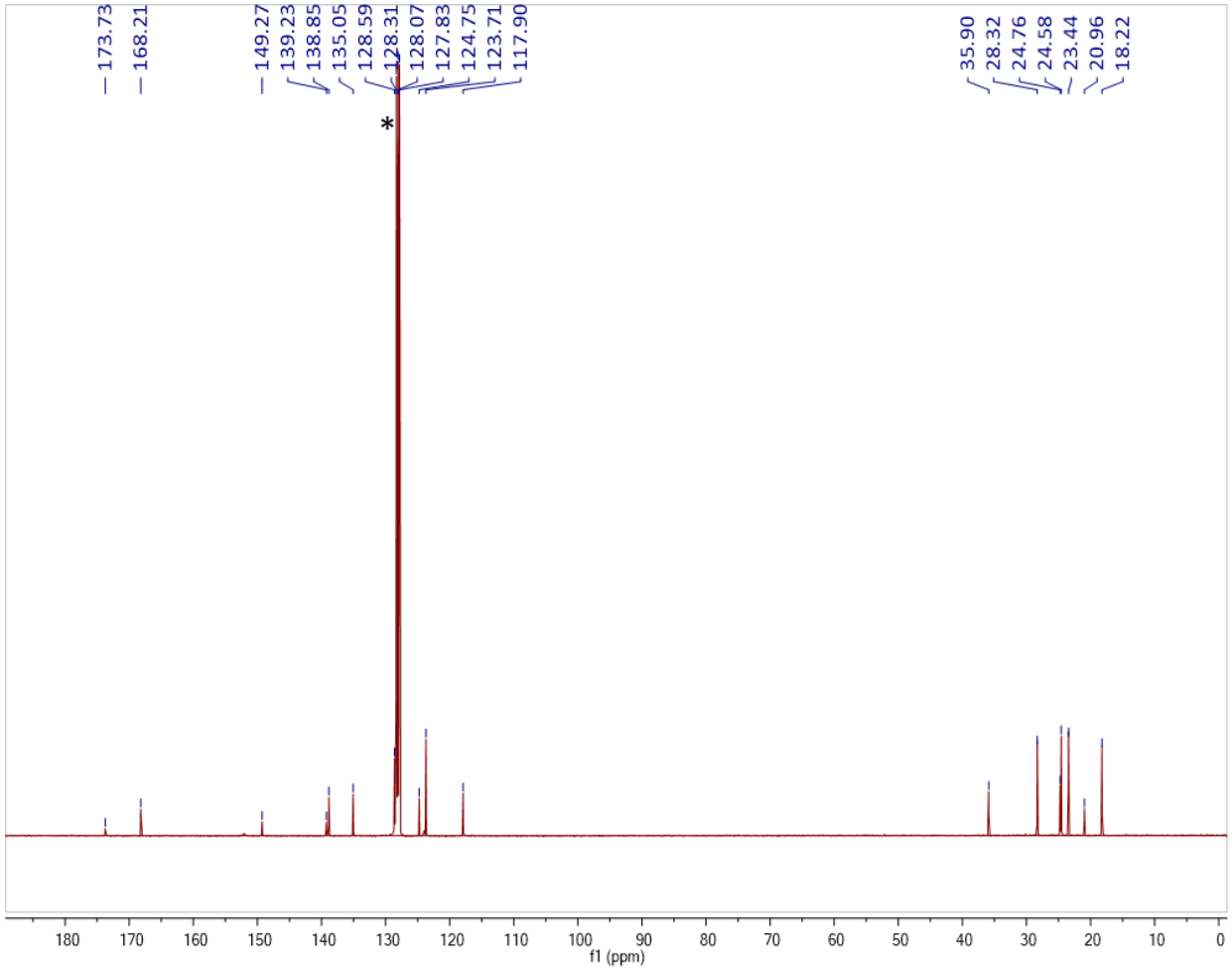

Figure S18. ^{13}C NMR spectrum of **L**$_1$Cu(2,4,6-$CNC_6H_2Me_3$) in C_6D_6 (100 MHz, 298 K). Solvent residual peaks are marked with an asterisk (*).

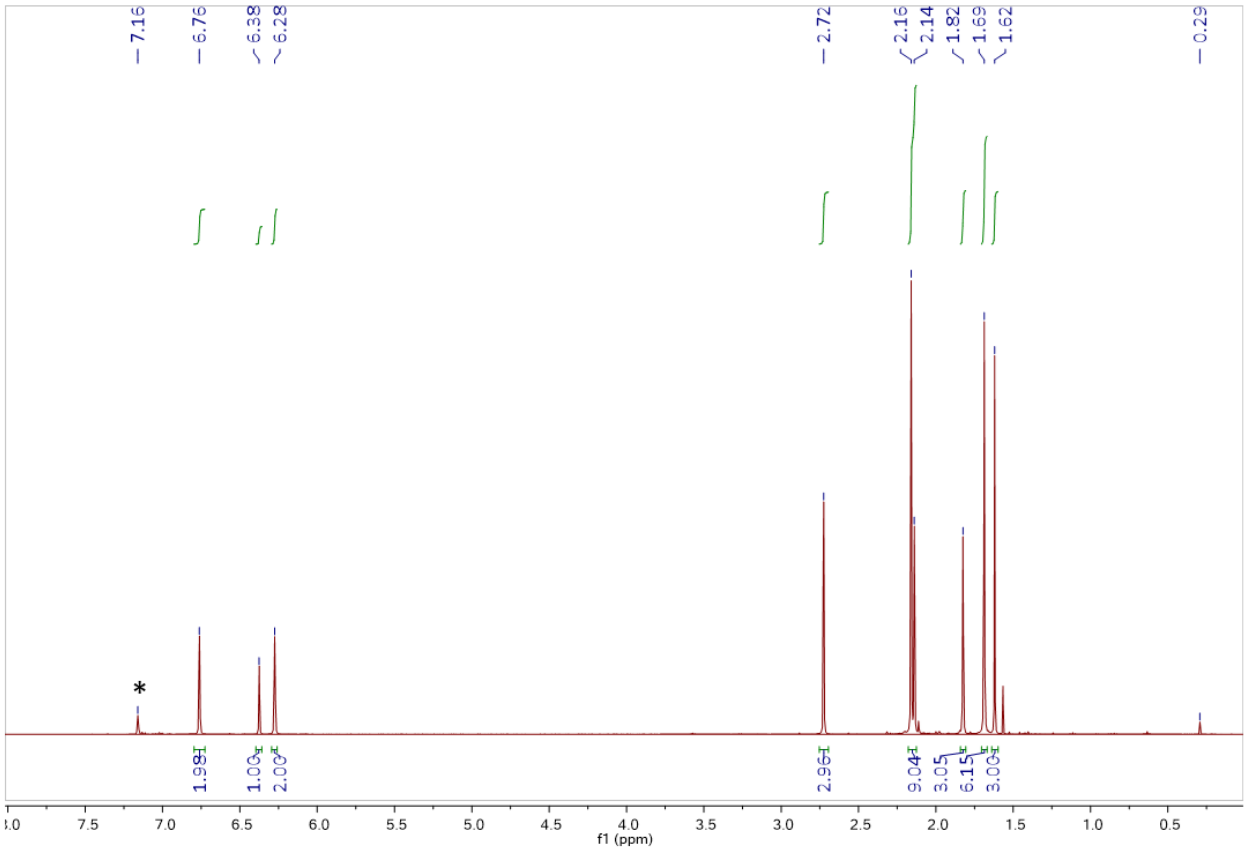

Figure S19. ^{1}H NMR spectrum of **L$_2$**Cu(2,4,6-CNC$_6$H$_2$Me$_3$) in C$_6$D$_6$ (400 MHz, 298 K). Solvent residual peaks are marked with an asterisk (*).

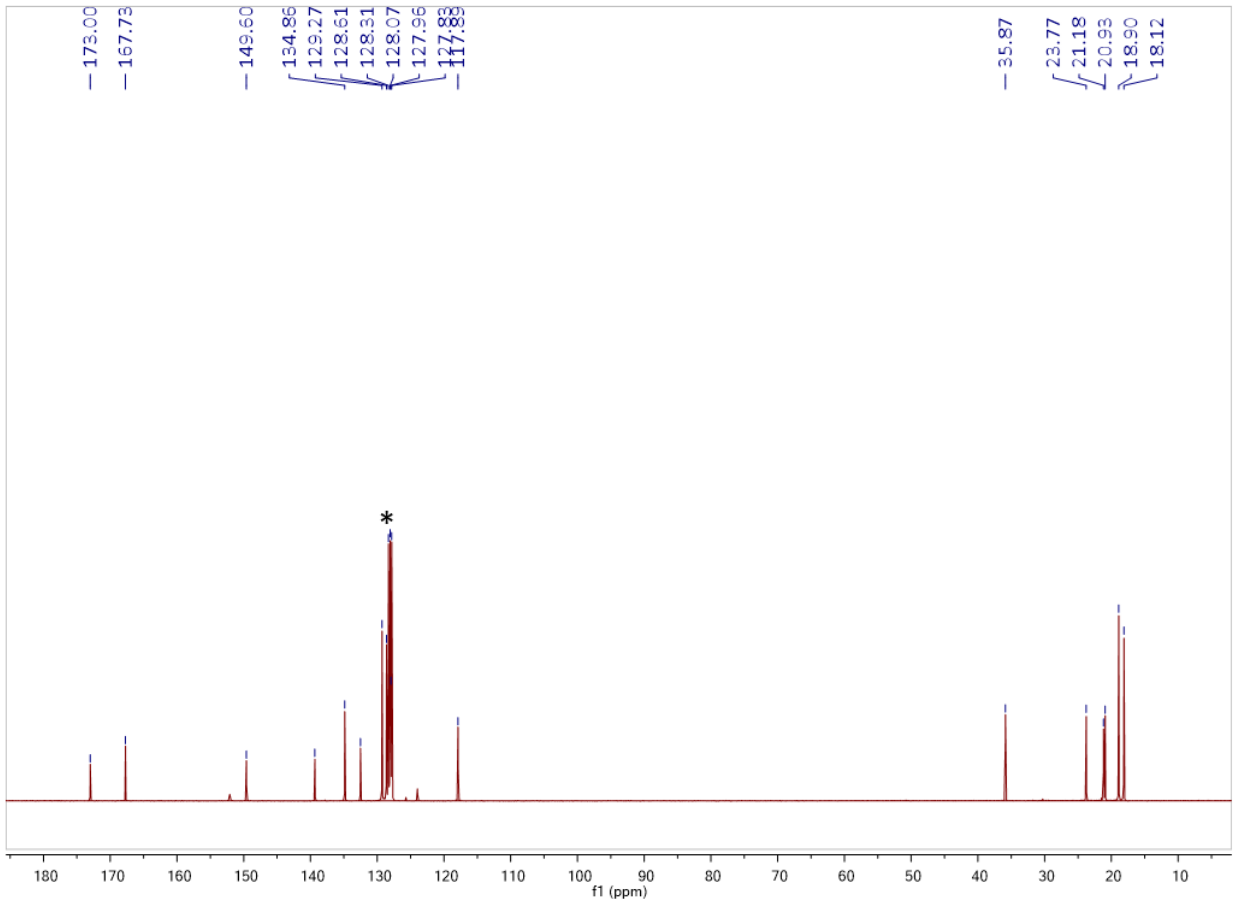

Figure S20. ^{13}C NMR spectrum of **L**$_2$Cu(2,4,6-CNC$_6$H$_2$Me$_3$) in C$_6$D$_6$ (100 MHz, 298 K). Solvent residual peaks are marked with an asterisk (*).

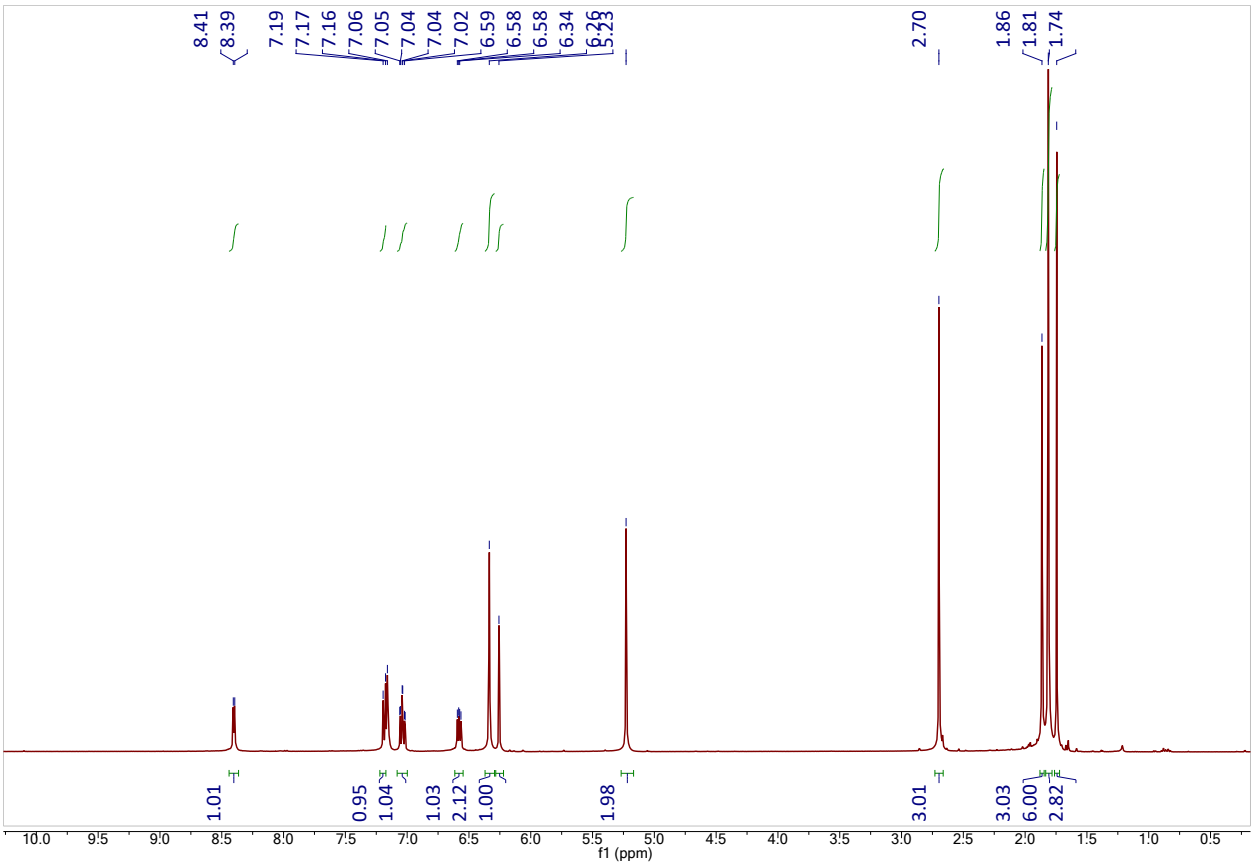

Figure S21. ^{1}H NMR spectrum of **L$_3$**Cu(2,4,6-CNC$_6$H$_2$Me$_3$) in C_6D_6 (400 MHz, 298 K).

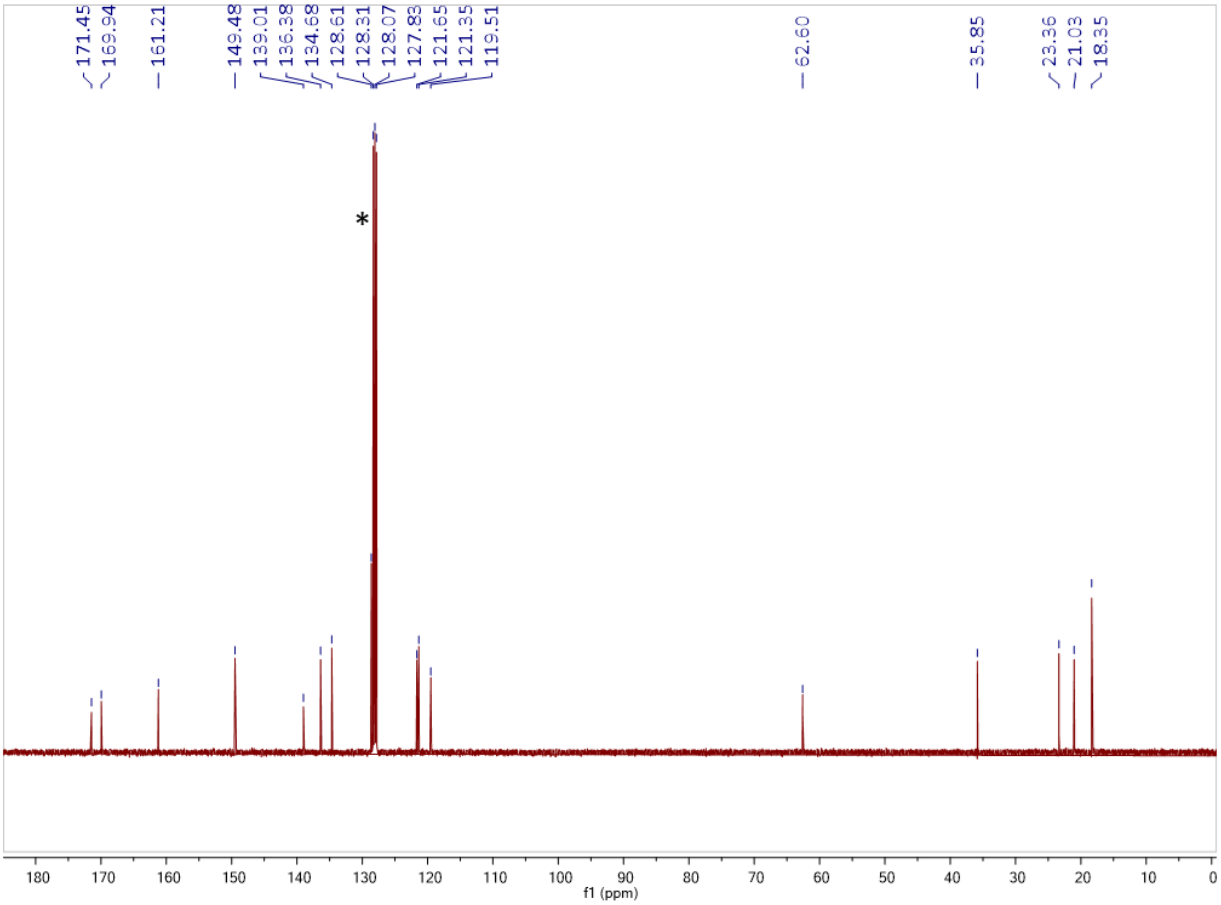

Figure S22. ^{13}C NMR spectrum of **L$_3$**Cu(2,4,6-CNC$_6$H$_2$Me$_3$) in C$_6$D$_6$ (100 MHz, 298 K). Solvent residual peaks are marked with an asterisk (*).

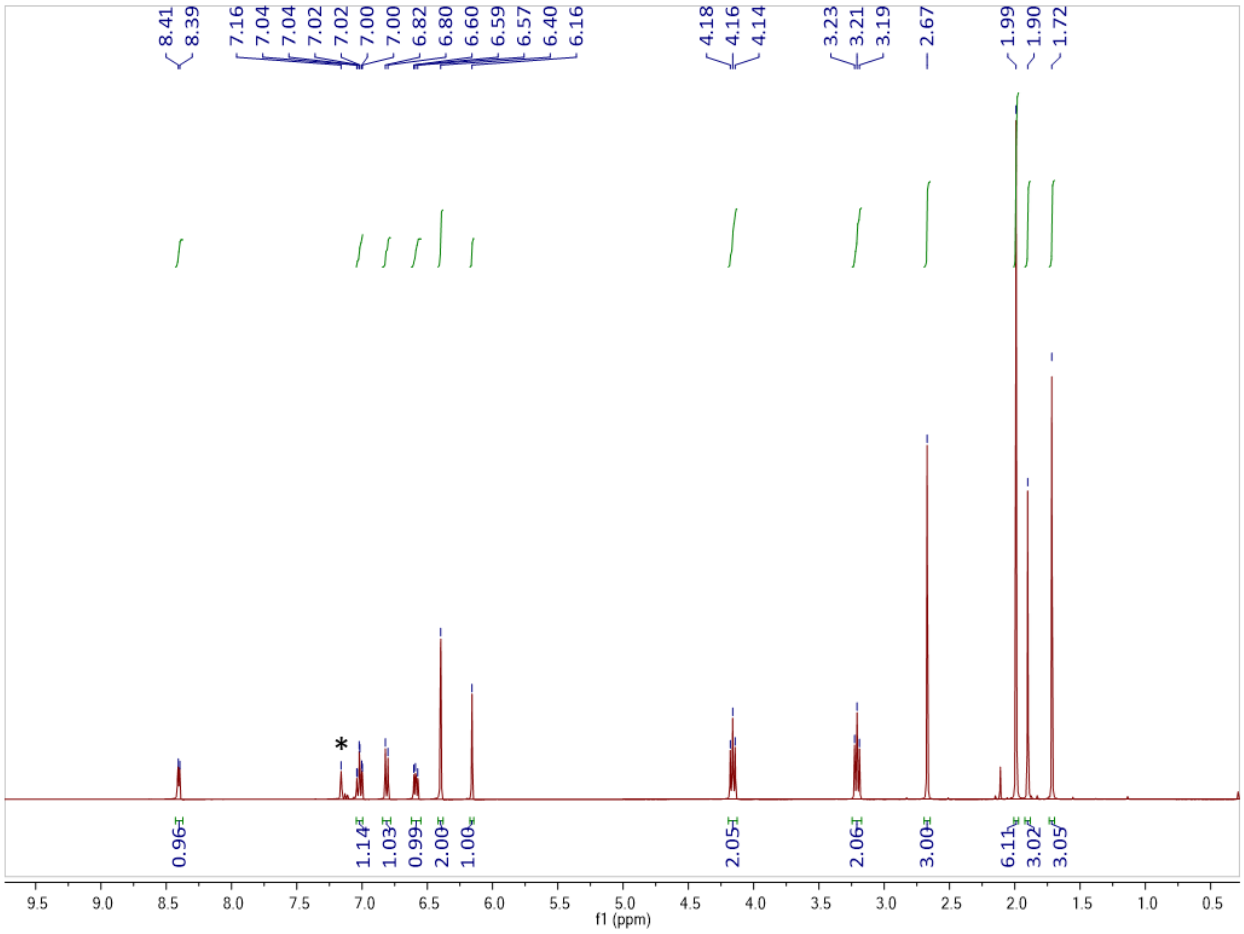

Figure S23. ^{1}H NMR spectrum of **L**$_4$Cu(2,4,6-CNC$_6$H$_2$Me$_3$) in C$_6$D$_6$ (400 MHz, 298 K). Solvent residual peaks are marked with an asterisk (*).

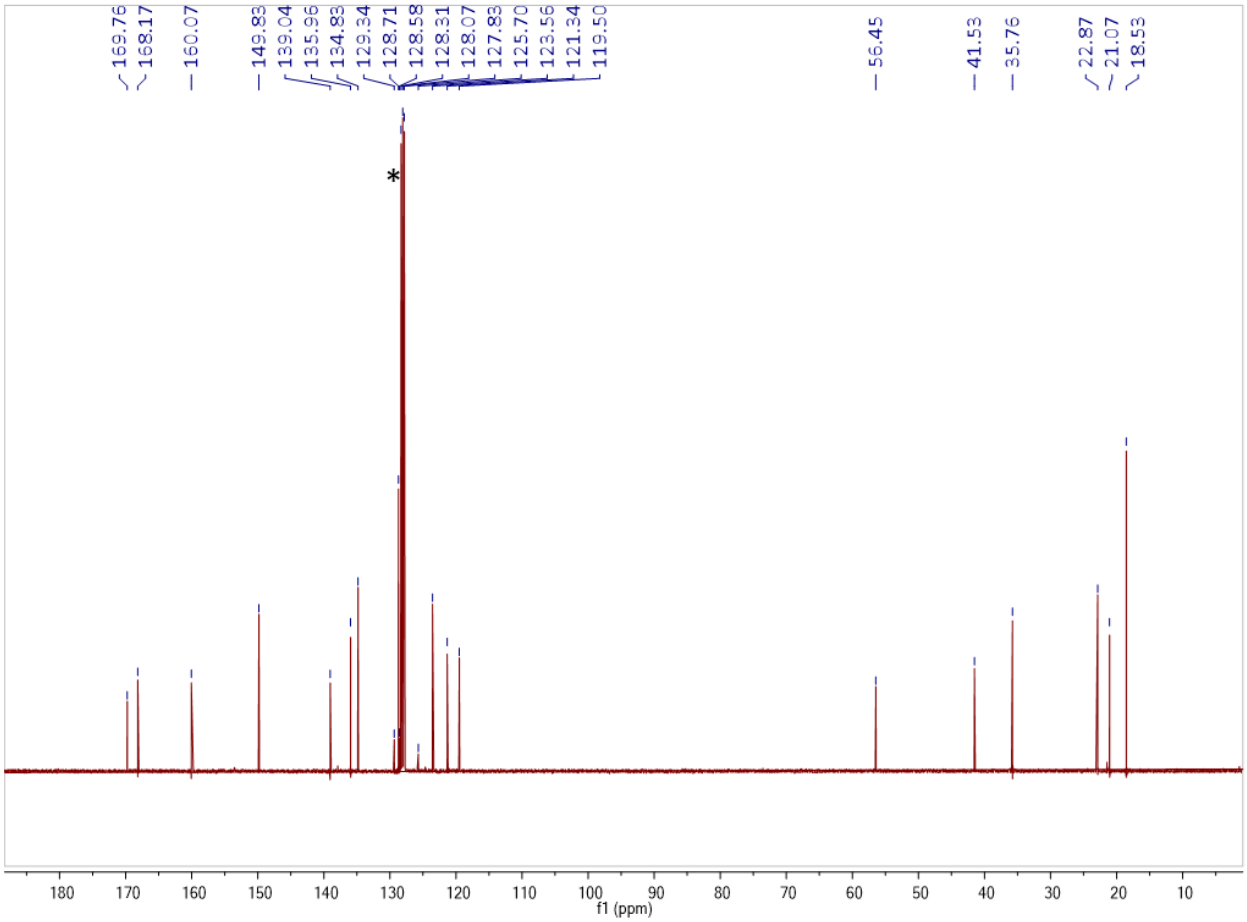

Figure S24. ^{13}C NMR spectrum of **L**$_4$Cu(2,4,6-CNC$_6$H$_2$Me$_3$) in C$_6$D$_6$ (100 MHz, 298 K). Solvent residual peaks are marked with an asterisk (*).

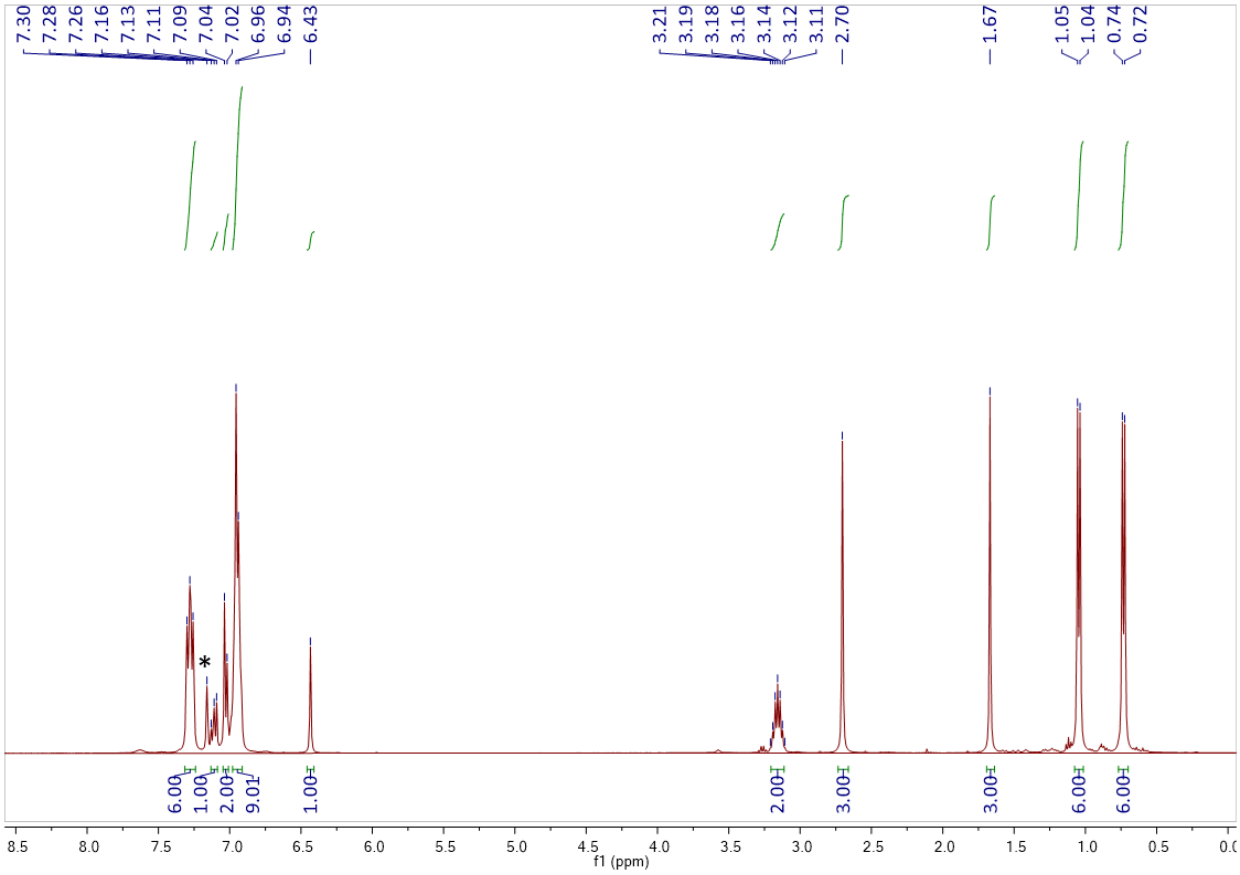

Figure S25. ^{1}H NMR spectrum of **L$_1$**Cu(PPh$_3$) in C_6D_6 (400 MHz, 298 K). Solvent residual peaks are marked with an asterisk (*).

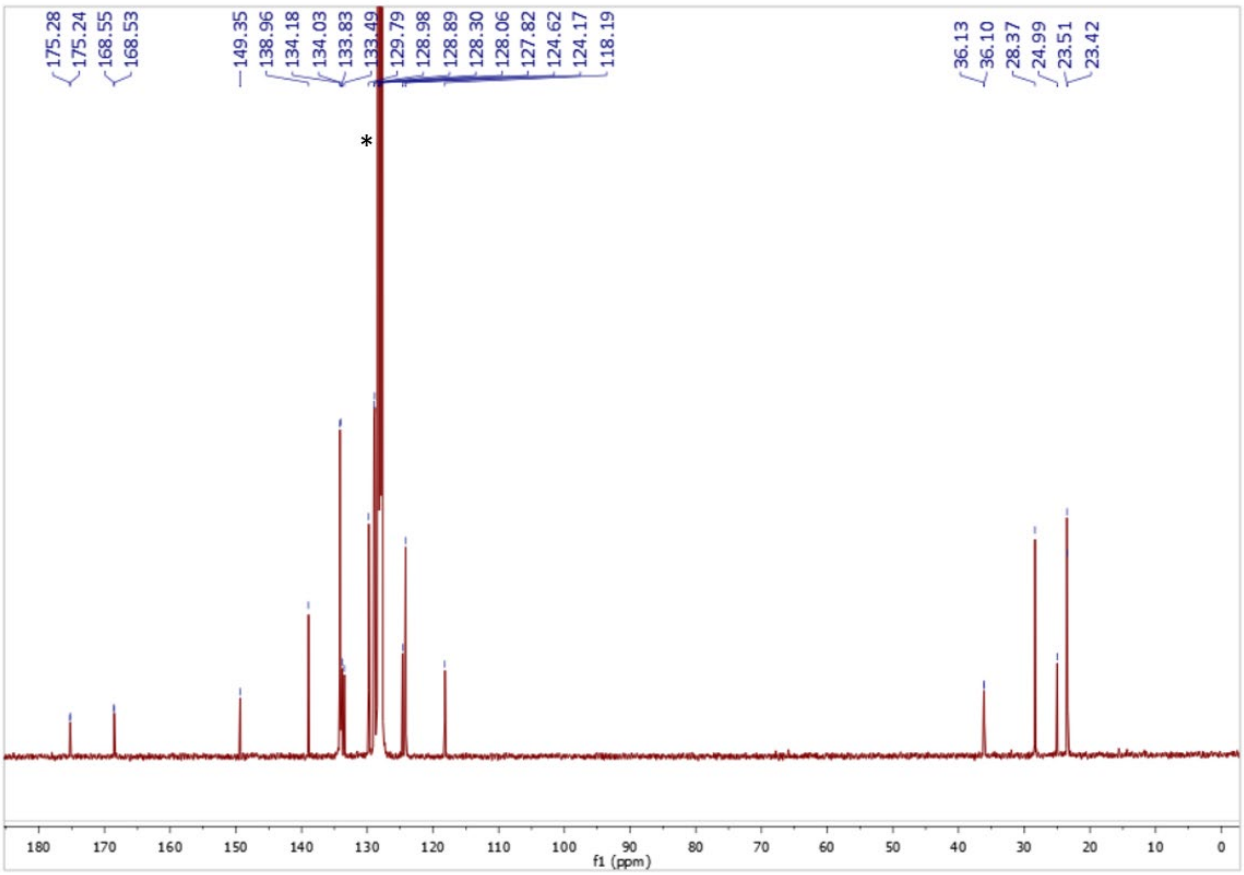

Figure S26. ^{13}C NMR spectrum of **L**$_1$Cu(PPh_3) in C_6D_6 (100 MHz, 298 K). Solvent residual peaks are marked with an asterisk (*).

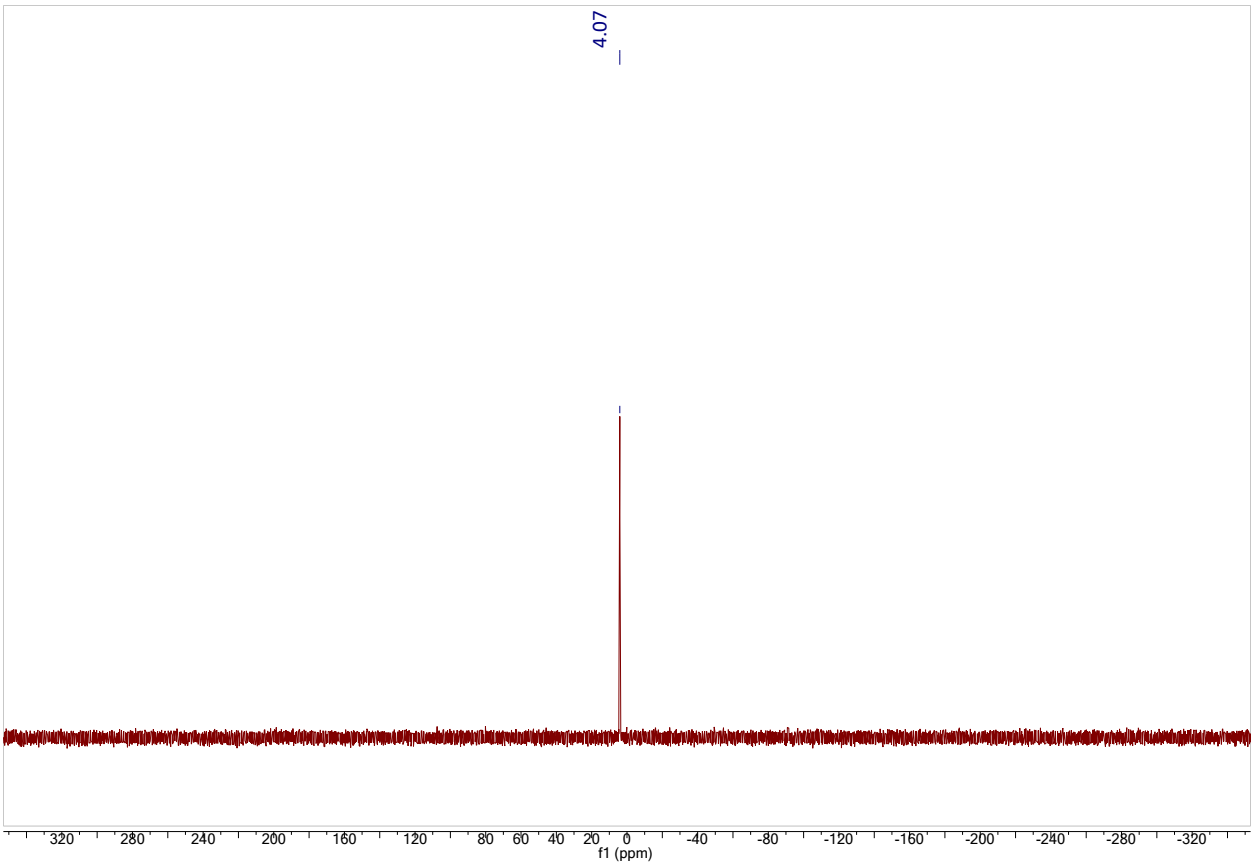

Figure S27. ^{31}P NMR spectrum of $\mathbf{L_1}Cu(PPh_3)$ in C_6D_6 (162 MHz, 298 K). Solvent residual peaks are marked with an asterisk (*).

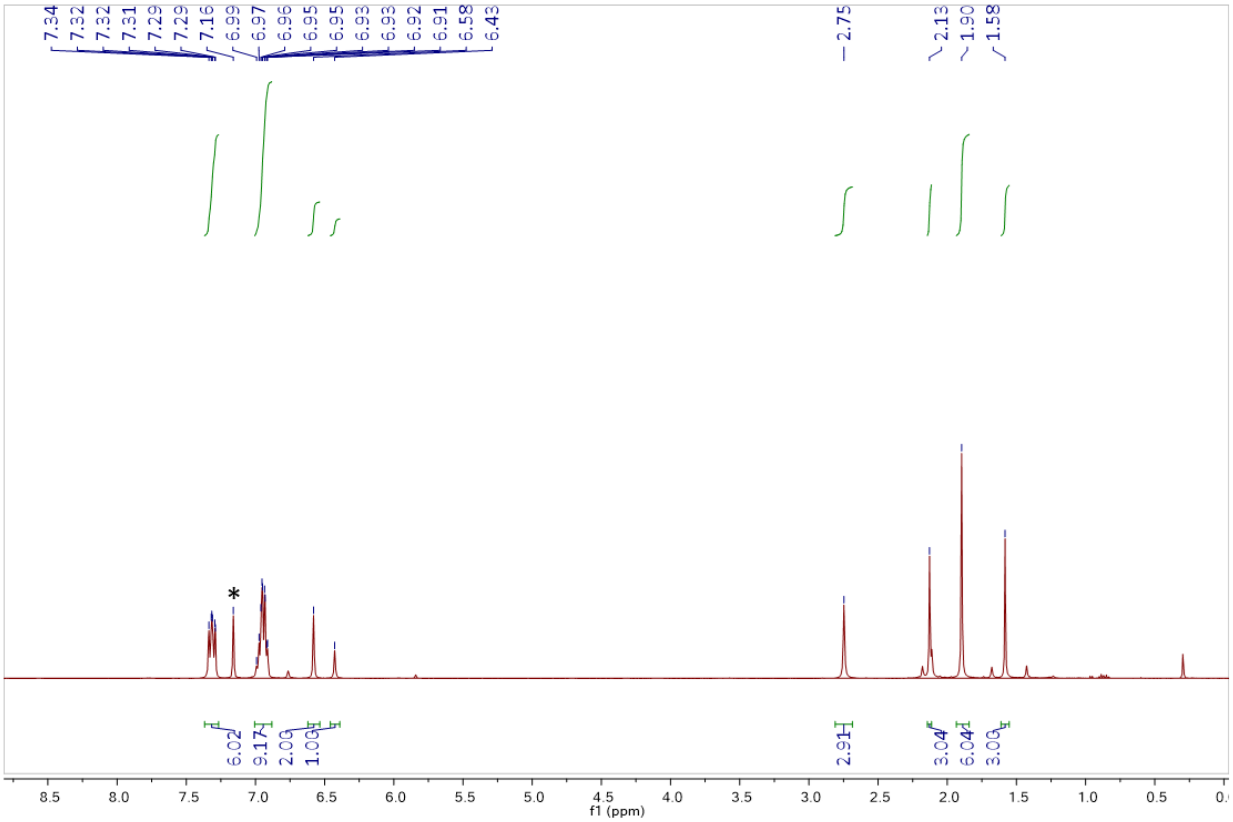

Figure S28. ^{1}H NMR spectrum of **L**$_2$Cu(PPh$_3$) in C_6D_6 (400 MHz, 298 K). Solvent residual peaks are marked with an asterisk (*).

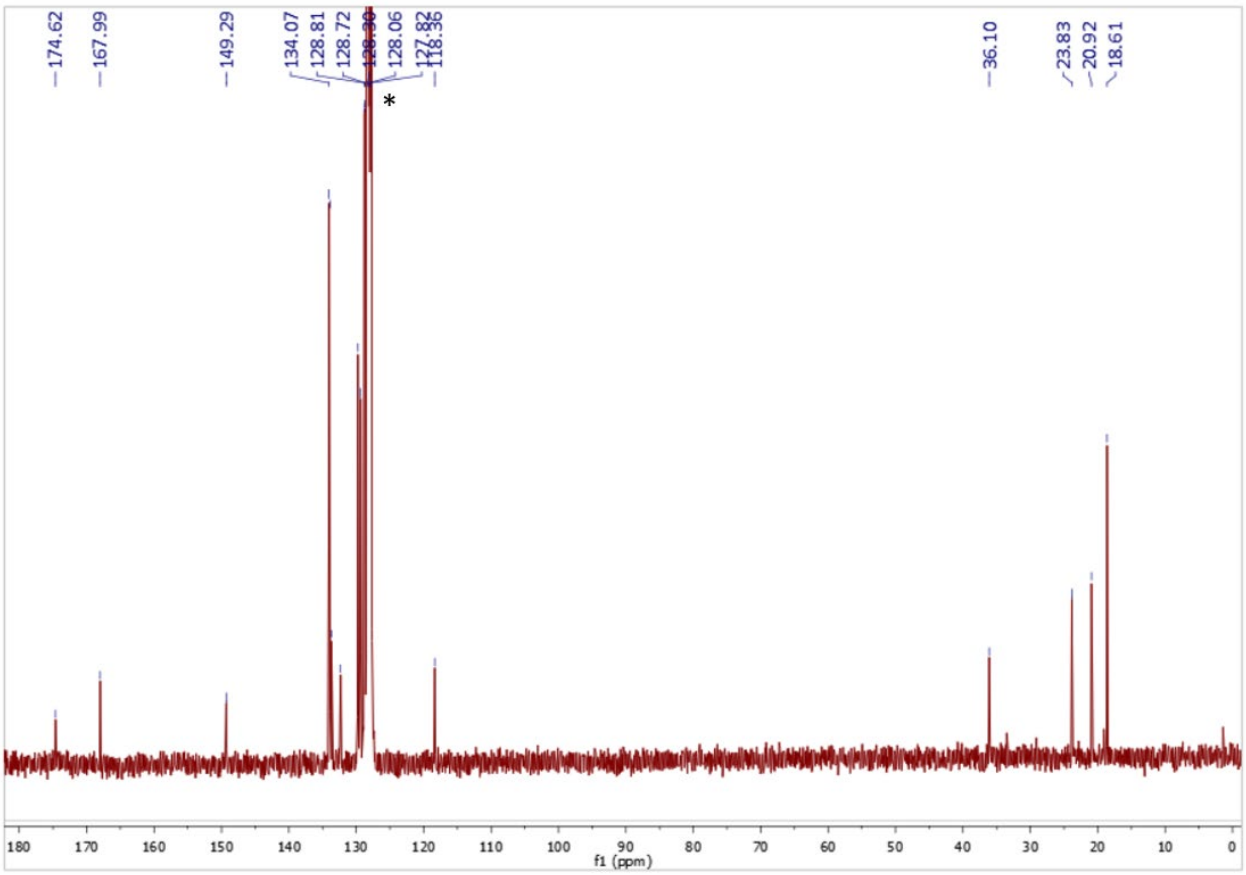

Figure S29. ^{13}C NMR spectrum of $\mathbf{L_2}Cu(PPh_3)$ in C_6D_6 (100 MHz, 298 K). Solvent residual peaks are marked with an asterisk (*).

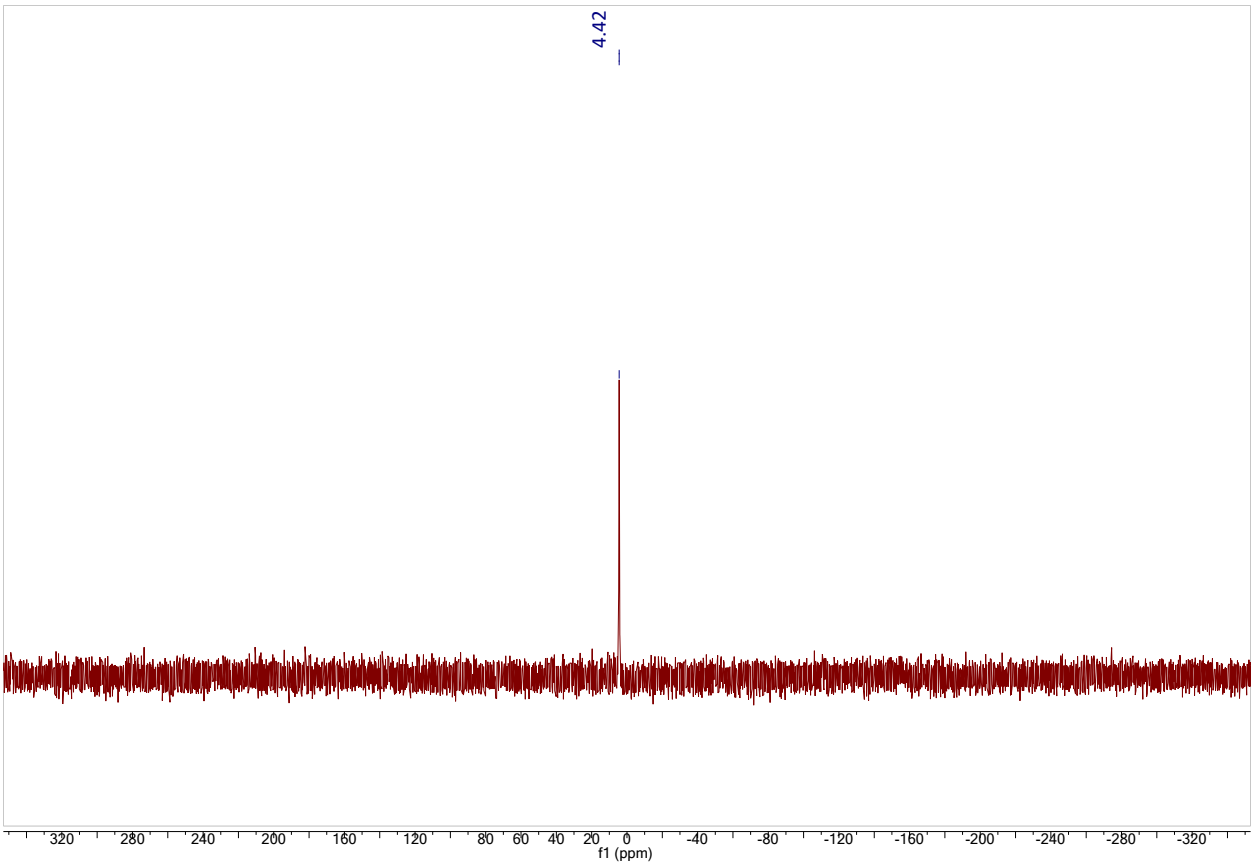

Figure S30. ^{31}P NMR spectrum of $\mathbf{L}_2Cu(PPh_3)$ in C_6D_6 (162 MHz, 298 K). Solvent residual peaks are marked with an asterisk (*).

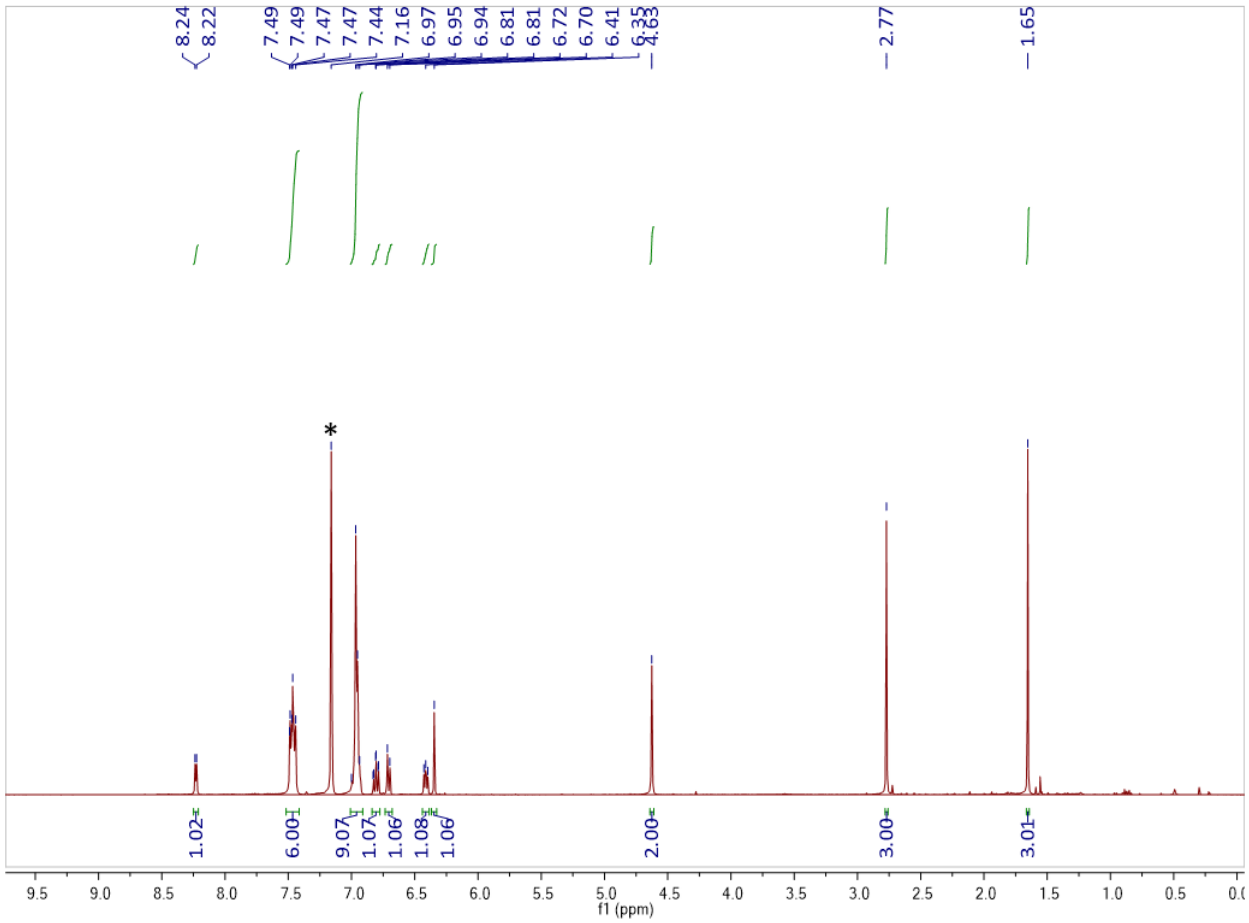

Figure S31. ^{1}H NMR spectrum of **L**$_3$Cu(PPh$_3$)in C_6D_6 (400 MHz, 298 K). Solvent residual peaks are marked with an asterisk (*).

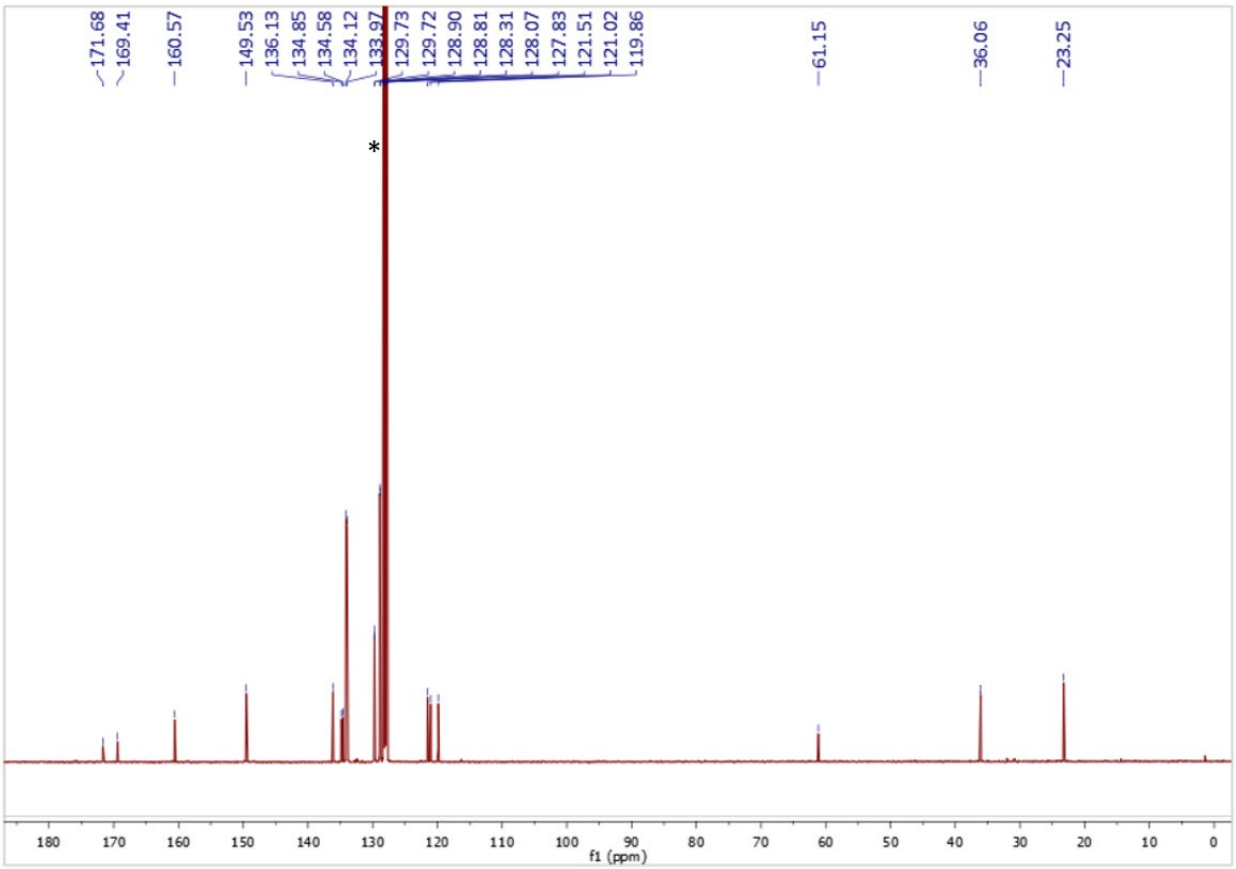

Figure S32. ^{13}C NMR spectrum of **L**$_3$Cu(PPh_3) in C_6D_6 (100 MHz, 298 K). Solvent residual peaks are marked with an asterisk (*).

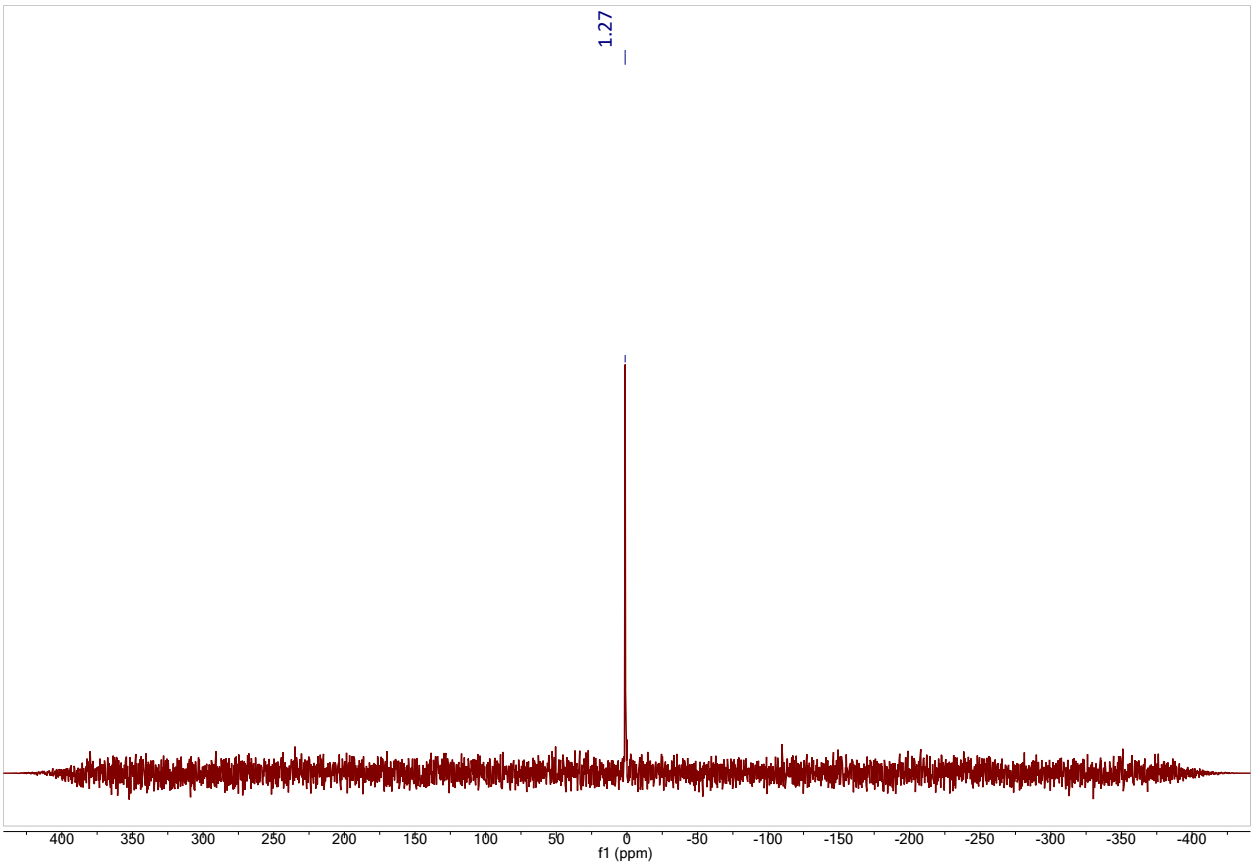

Figure S33. ^{31}P NMR spectrum of $\mathbf{L_3}Cu(PPh_3)$ in C_6D_6 (162 MHz, 298 K). Solvent residual peaks are marked with an asterisk (*).

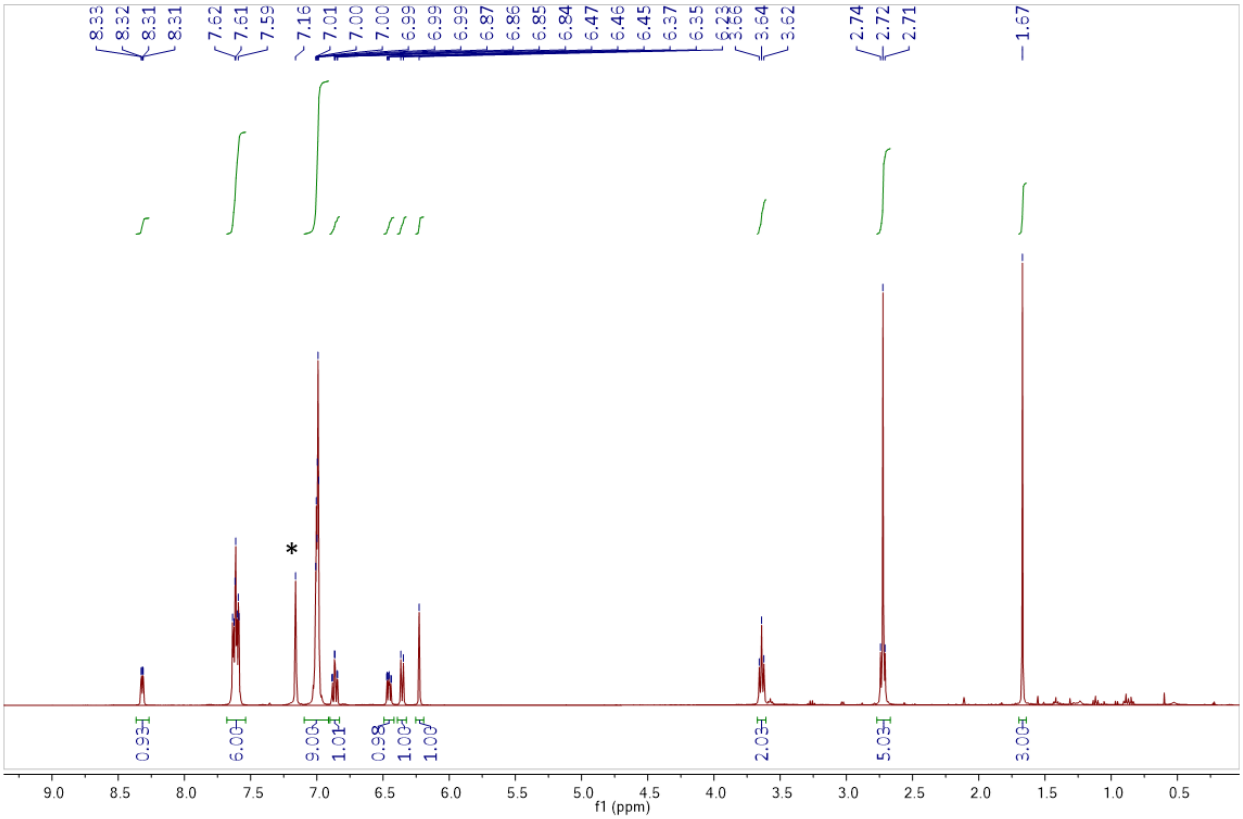

Figure S34. ^{1}H NMR spectrum of **L**$_4$Cu(PPh$_3$) in C_6D_6 (400 MHz, 298 K). Solvent residual peaks are marked with an asterisk (*).

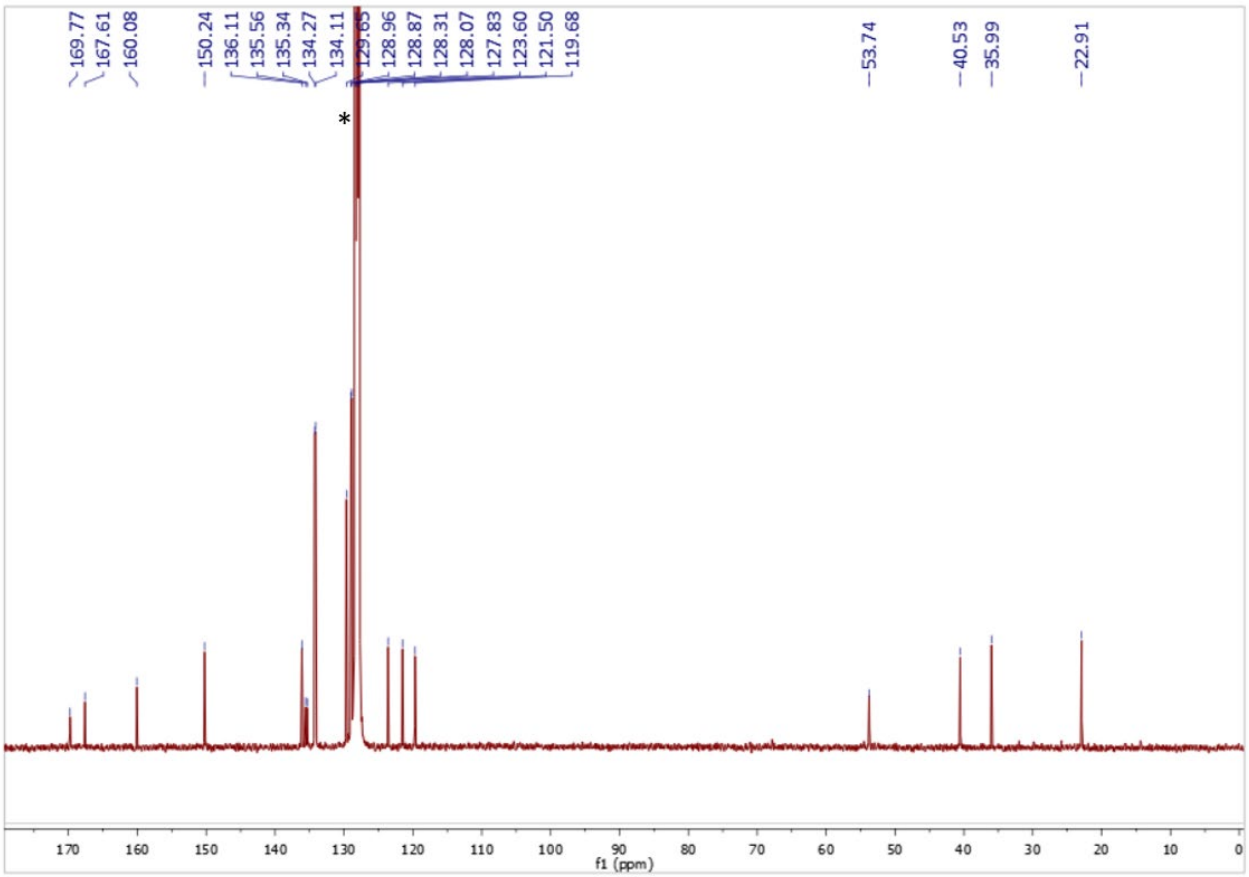

Figure S35. ^{13}C NMR spectrum of **L**$_4$Cu(PPh_3) in C_6D_6 (100 MHz, 298 K). Solvent residual peaks are marked with an asterisk (*).

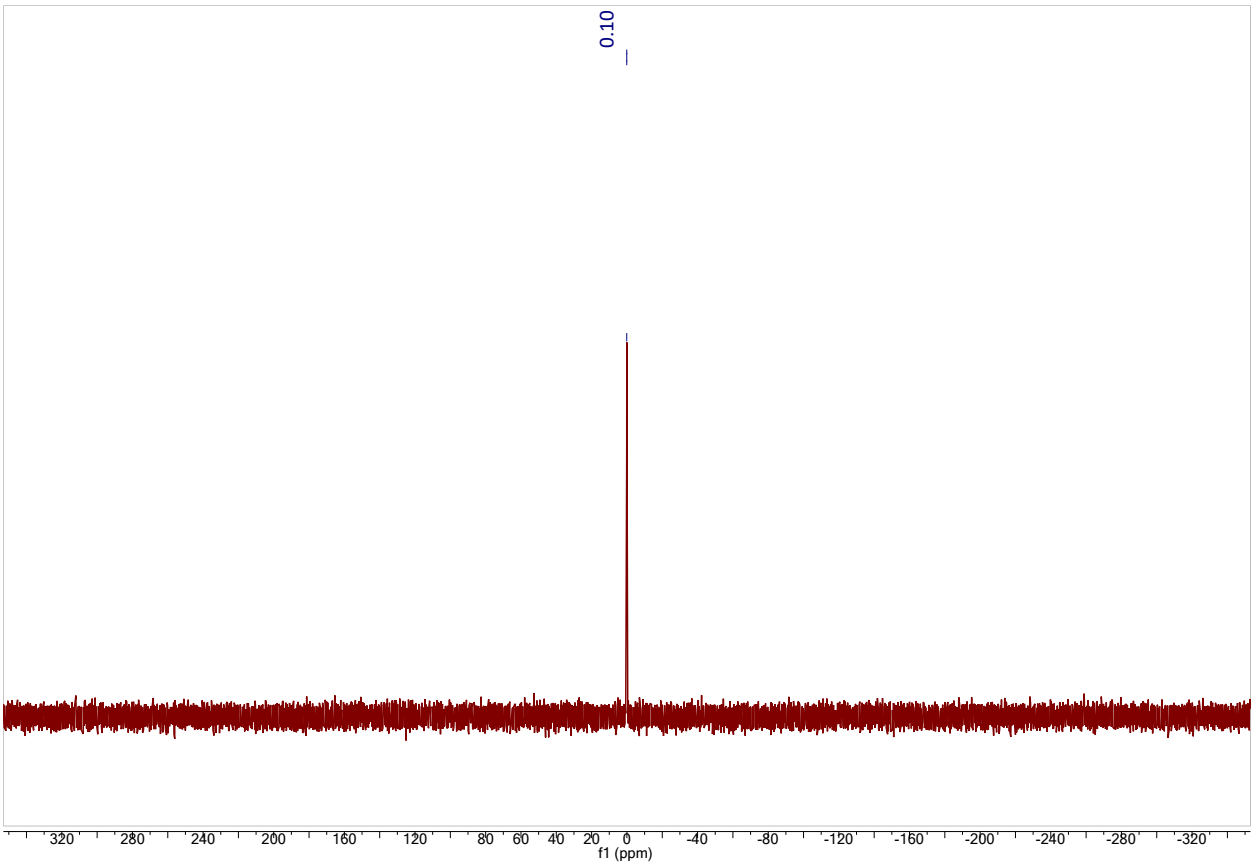

Figure S36. ^{31}P NMR spectrum of $\mathbf{L_4}Cu(PPh_3)$ in C_6D_6 (162 MHz, 298 K). Solvent residual peaks are marked with an asterisk (*).

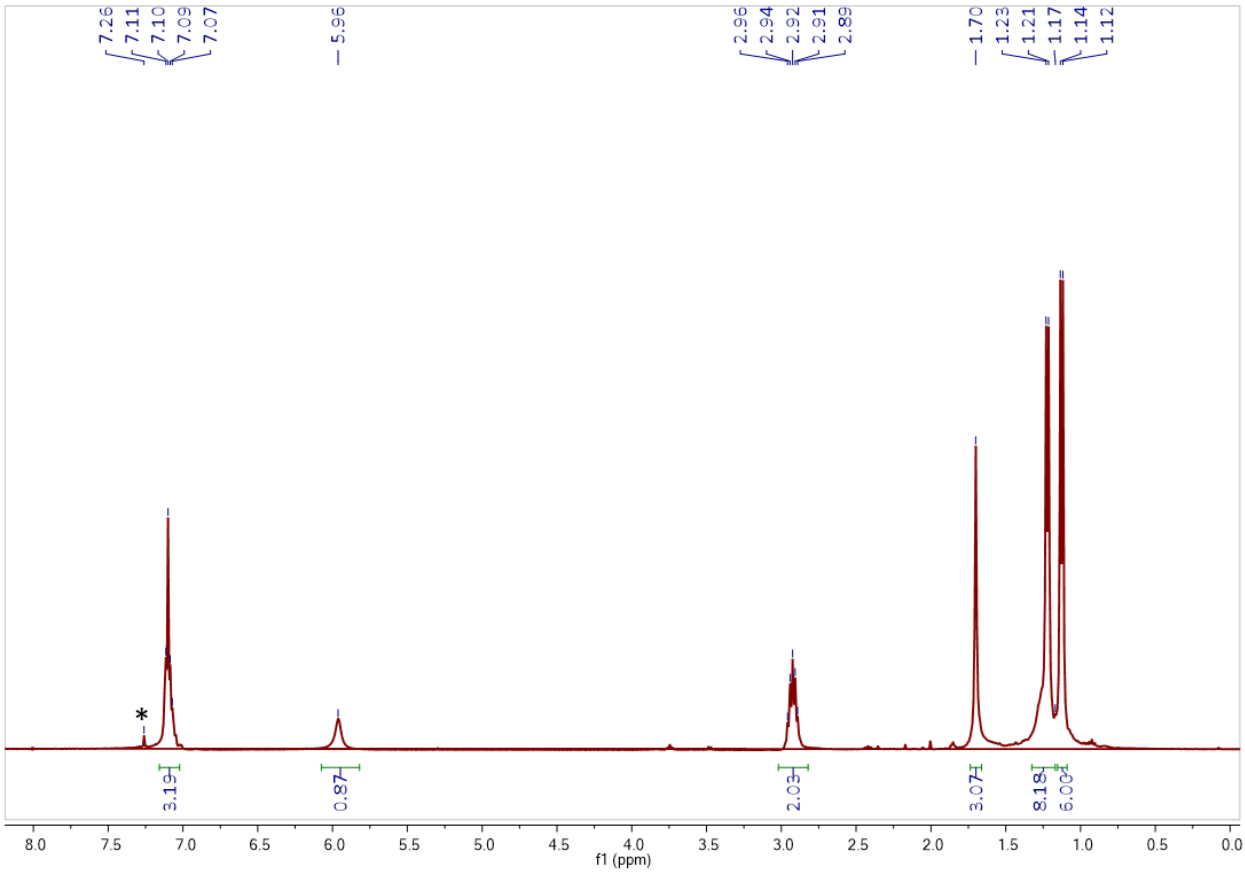

Figure S37. ^{1}H NMR spectrum of **L$_1$**Cu-CO in $CDCl_3$ (400 MHz, 298 K). Solvent residual peaks are marked with an asterisk (*).

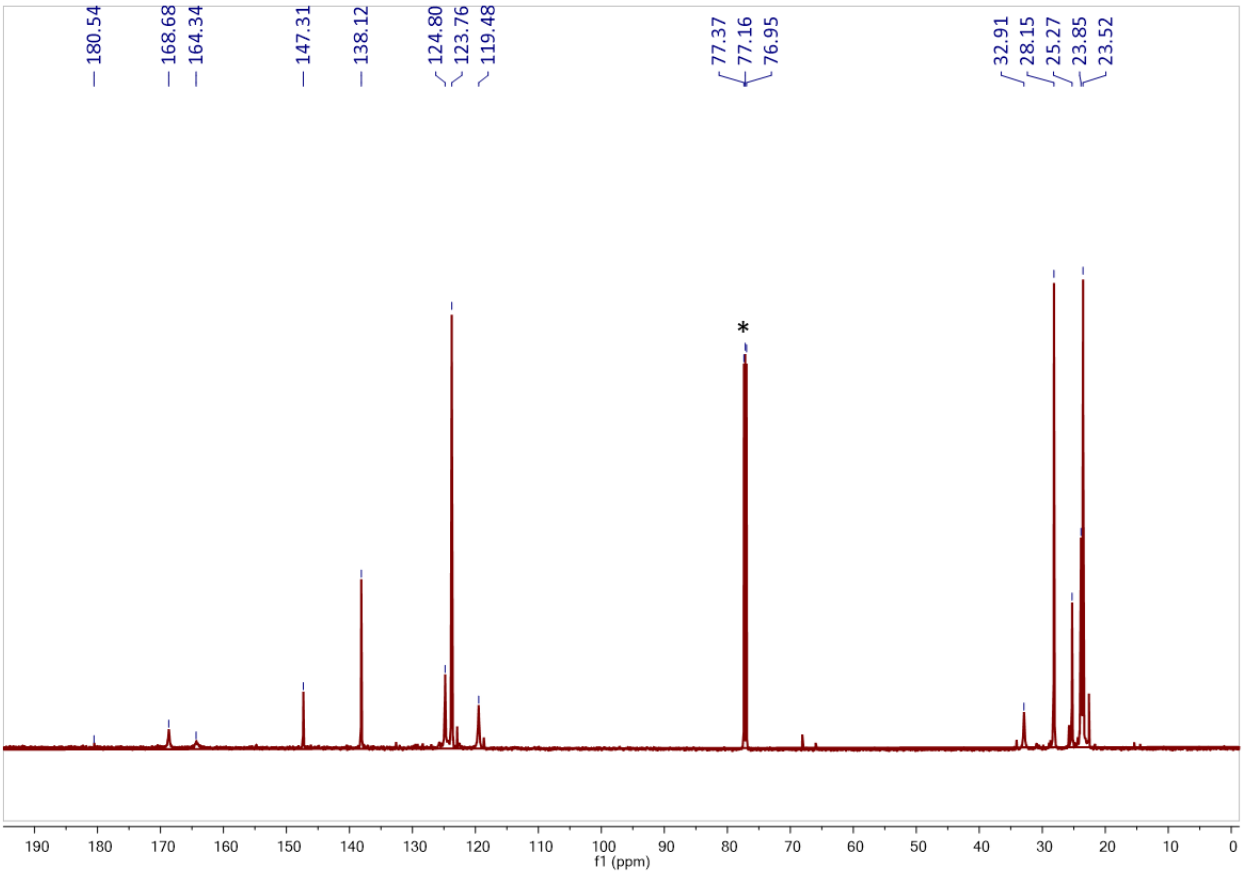

Figure S38. ^{13}C NMR spectrum of **L**$_1$Cu-CO in $CDCl_3$ (100 MHz, 298 K). Solvent residual peaks are marked with an asterisk (*).

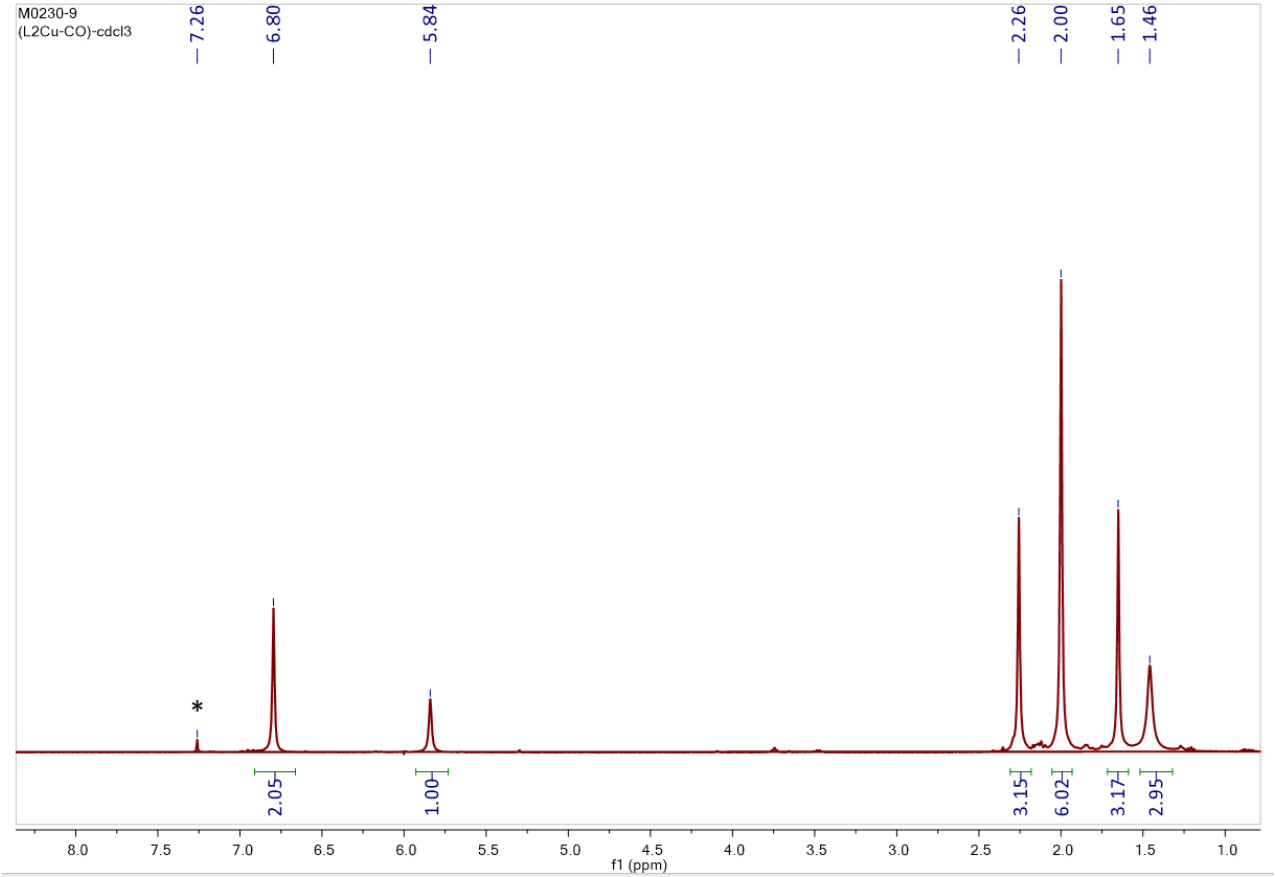

Figure S39. ^{1}H NMR spectrum of **L**$_2$Cu-CO in $CDCl_3$ (400 MHz, 298 K). Solvent residual peaks are marked with an asterisk (*).

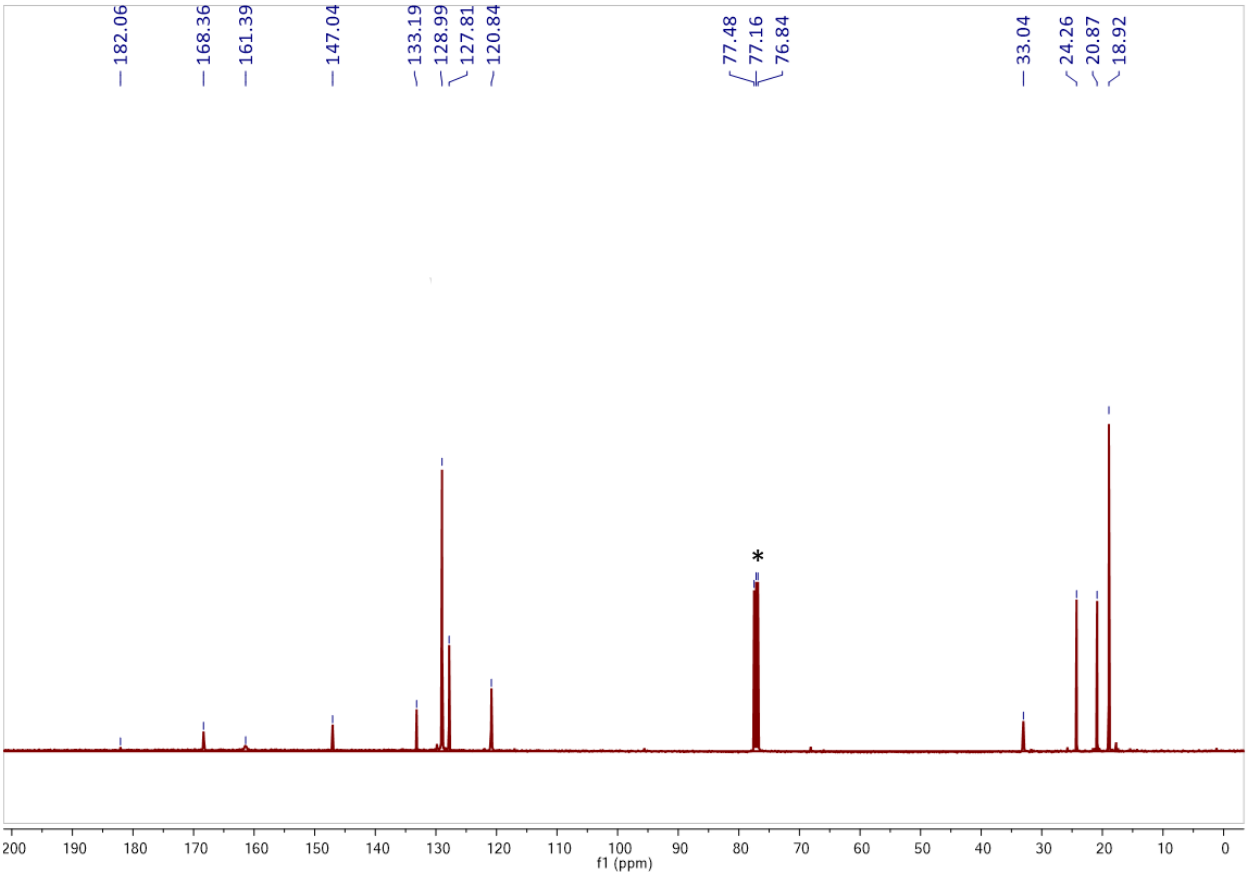

Figure S40. ^{13}C NMR spectrum of **L**$_2$Cu-CO in $CDCl_3$ (400 MHz, 298 K). Solvent residual peaks are marked with an asterisk (*).

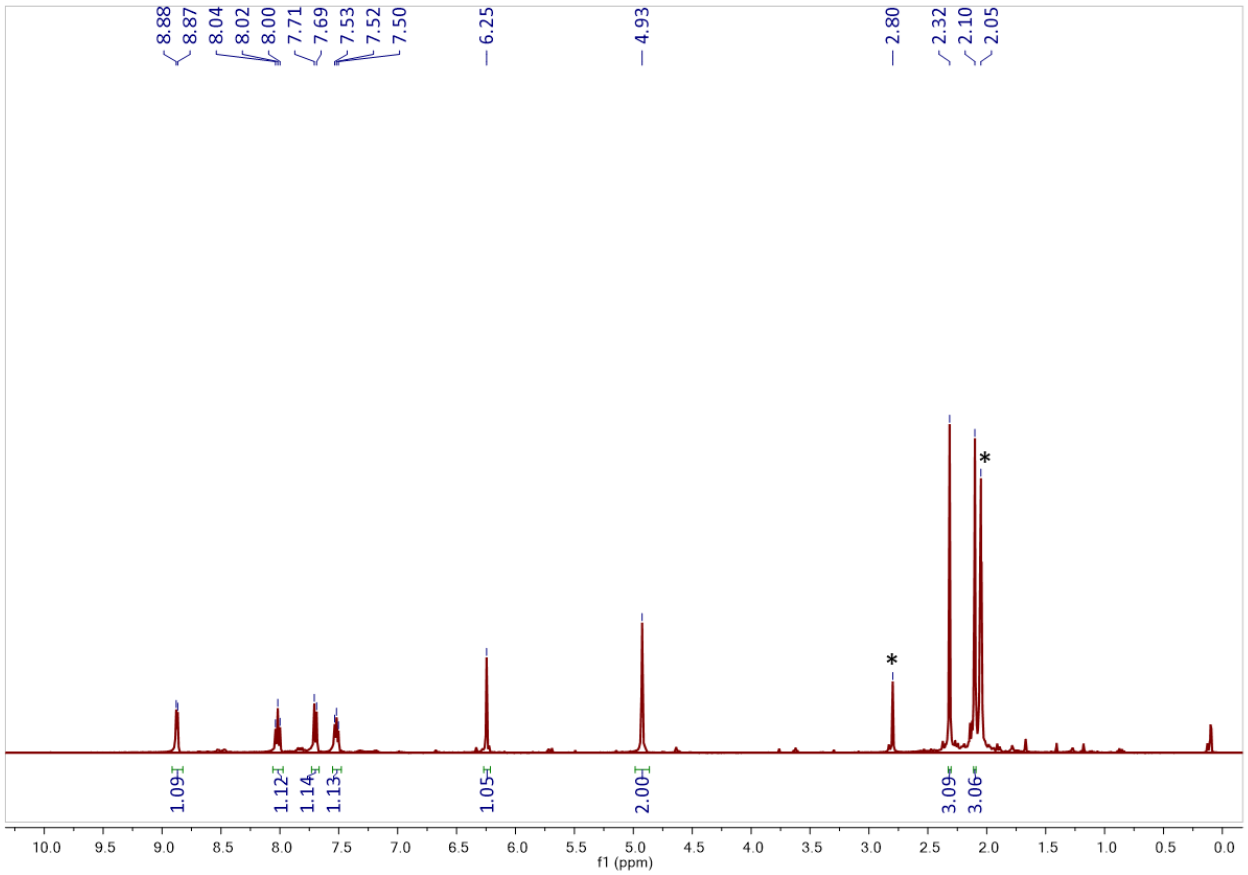

Figure S41. ^{1}H NMR spectrum of **L$_3$**Cu-CO in Acetone-D$_6$ (400 MHz, 298 K). Solvent residual peaks are marked with an asterisk (*).

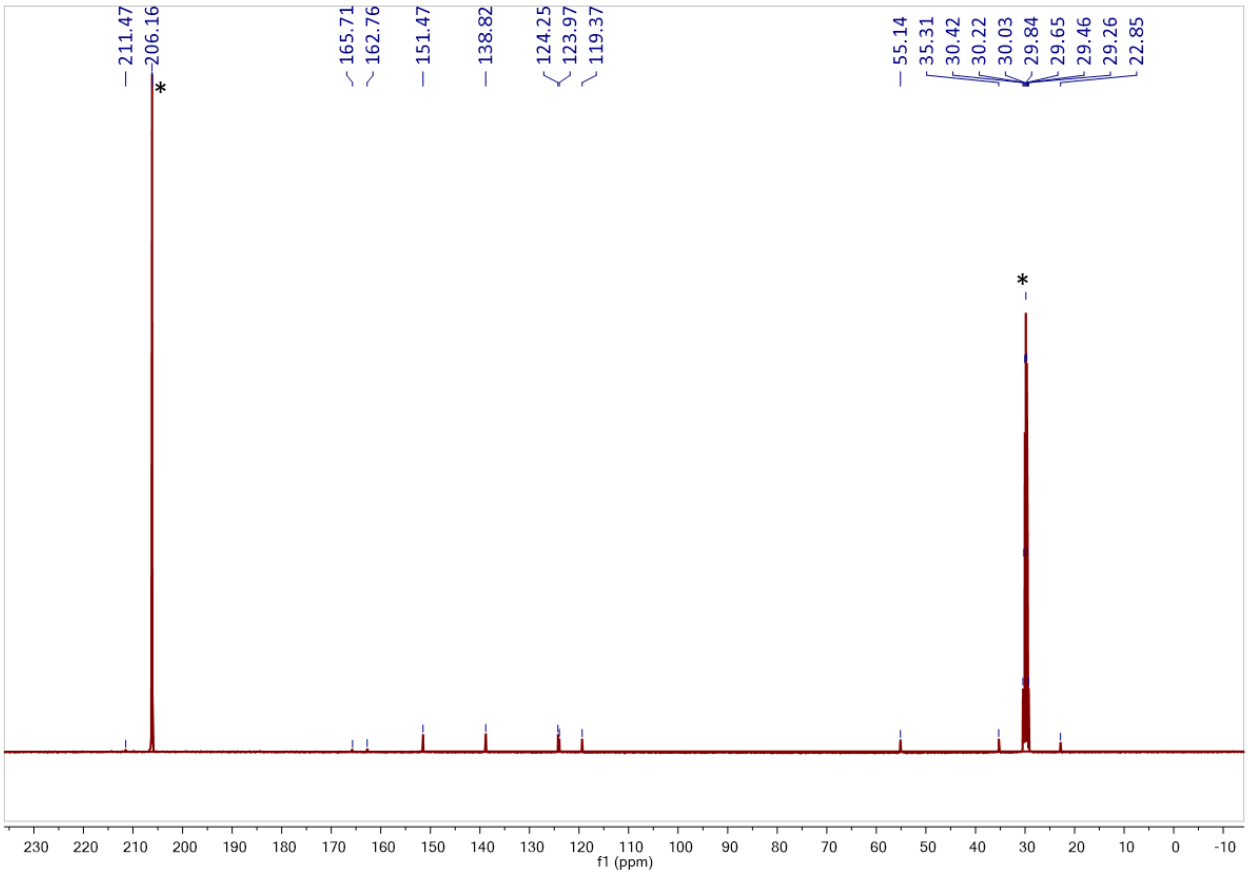

Figure S42. ^{13}C NMR spectrum of **L**$_3$Cu-CO in Acetone-D_6 (100 MHz, 298 K). Solvent residual peaks are marked with an asterisk (*).

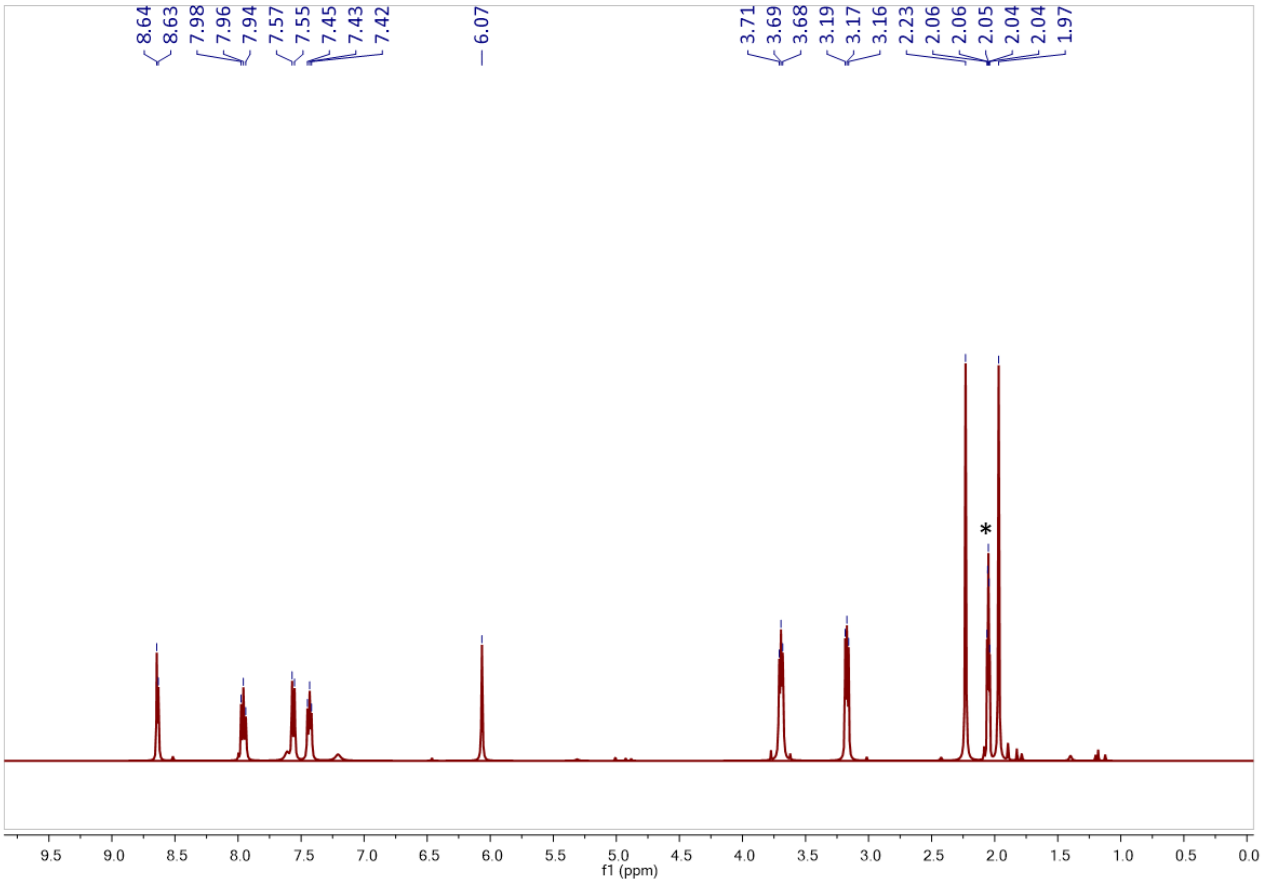

Figure S43. ^{1}H NMR spectrum of **L**$_4$Cu-CO in Acetone-D$_6$ (400 MHz, 298 K). Solvent residual peaks are marked with an asterisk (*).

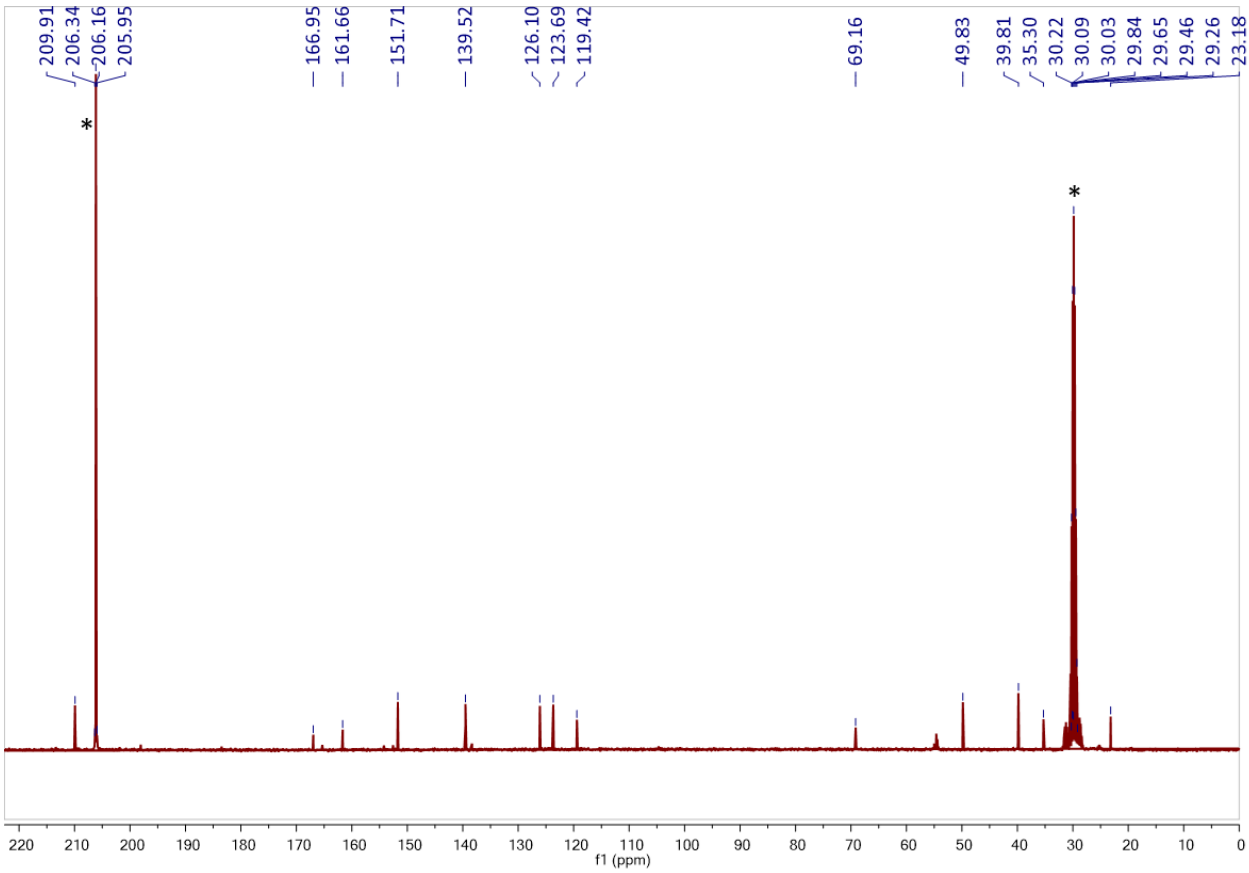

Figure S44. ^{13}C NMR spectrum of **L**$_4$Cu-CO in Acetone-D_6 (100 MHz, 298 K). Solvent residual peaks are marked with an asterisk (*).

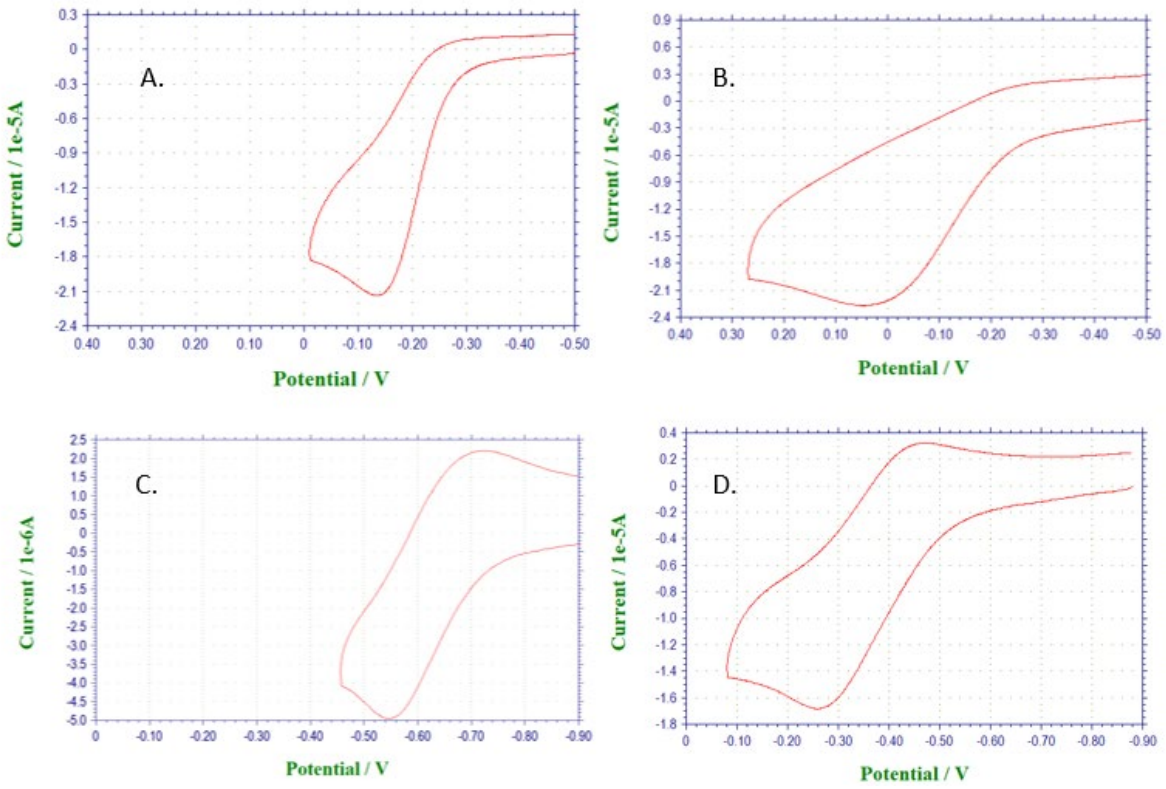

Figure S45. Cyclic voltammetry diagrams of (A) $[\mathbf{L_1}Cu]_3$, (B) $[\mathbf{L_2}Cu]_3$, (C) $\mathbf{L_3}Cu$, and (D) $\mathbf{L_4}Cu$ in 10^{-4} M MeCN solutions using 0.1 M $(Bu_4N)(PF_6)$ as supporting electrolyte, referenced to $Fc^{+/0}$.

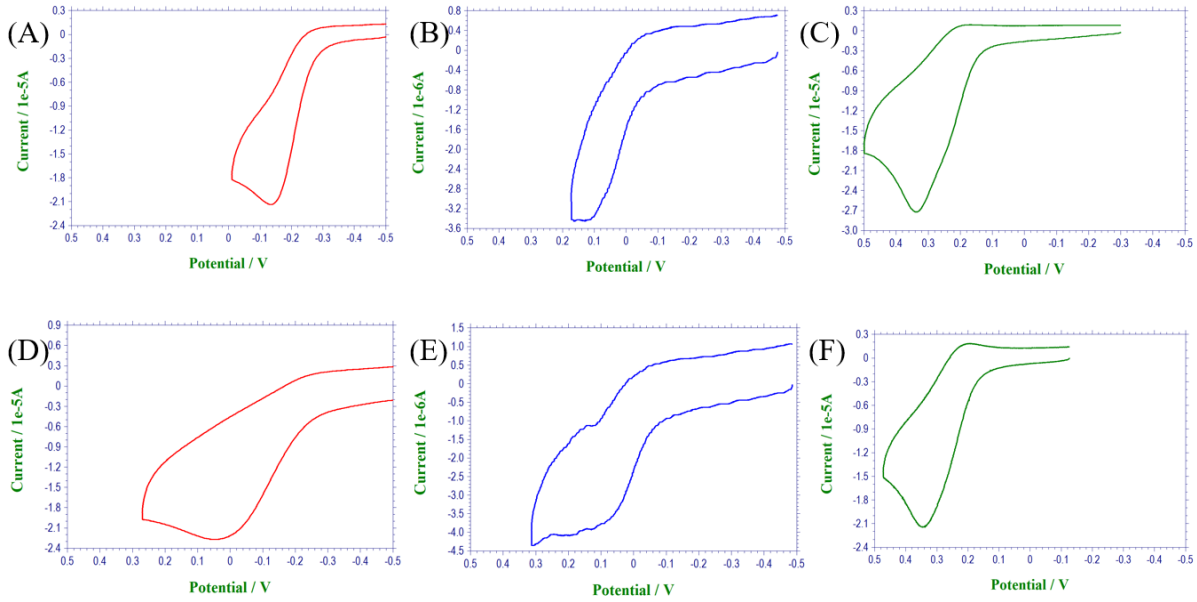

Figure S46. Cyclic voltammetry diagrams correspond to two SN chelator copper complexes with 10^{-4} M solutions of [**L**$_1$Cu]$_3$ in (A) CH_3CN, (B) CH_2Cl_2, (C) CH_3NO_2 respectively and [**L**$_2$Cu]$_3$ in (D) CH_3CN, (E) CH_2Cl_2, (F) CH_3NO_2 respectively using 0.1 M $(Bu_4N)(PF_6)$ as supporting electrolyte, referenced to $Fc^{+/0}$.

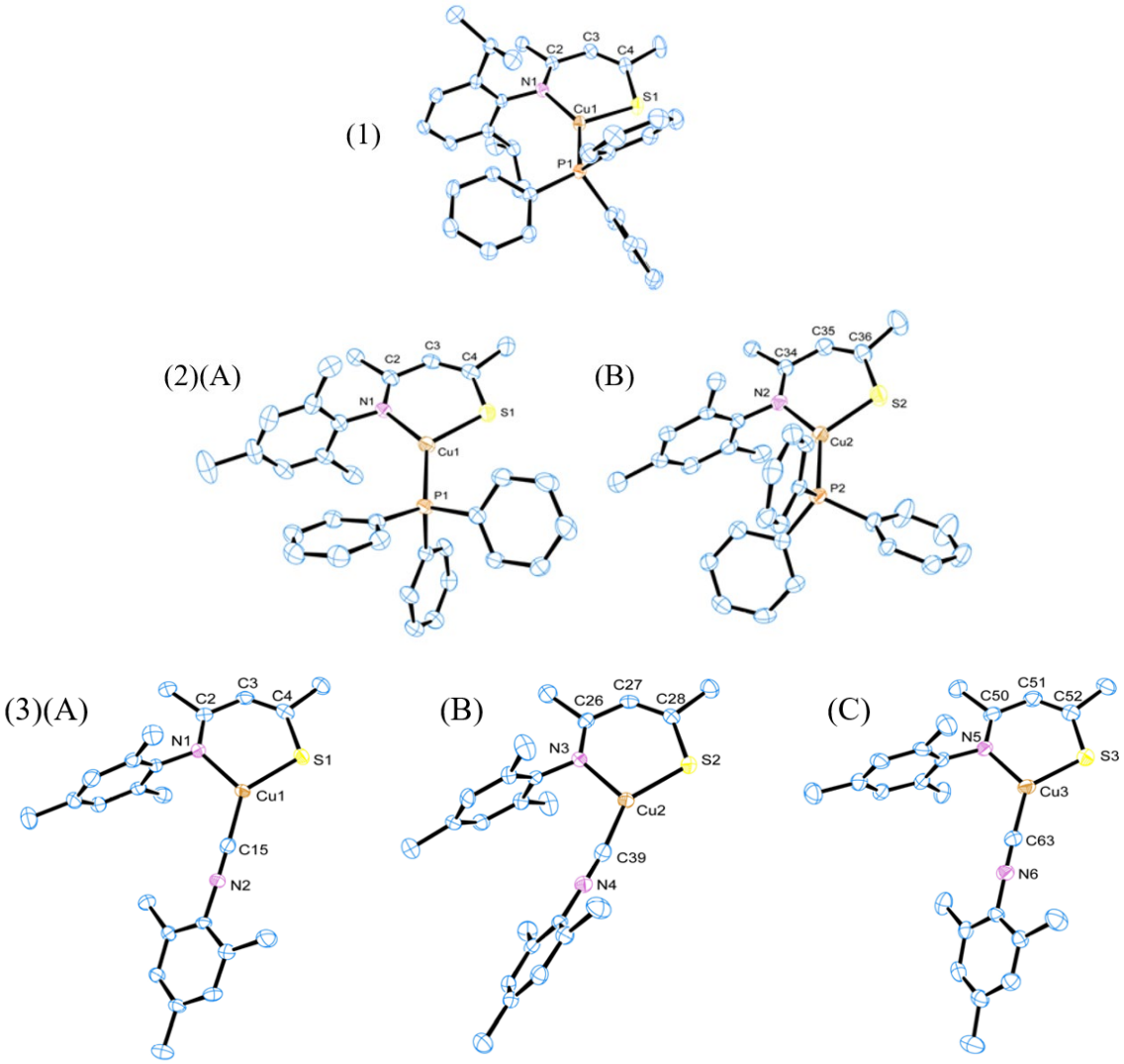

Figure S47. (1) ORTEP X-ray structure of $\mathbf{L_1}Cu(PPh_3)$ (2) ORTEP X-ray structures of two independent molecules of $\mathbf{L_2}CuPPh_3$ (a) and (b) similar to each other present in same unit cell (3) ORTEP X-ray structures of three independent molecules of $\mathbf{L_2}Cu(2,4,6\text{-}CNC_6H_2Me_3)$ a, b, and c similar to each other present in same unit cell at the 50% probability level. Hydrogen atoms are not shown for clarity.

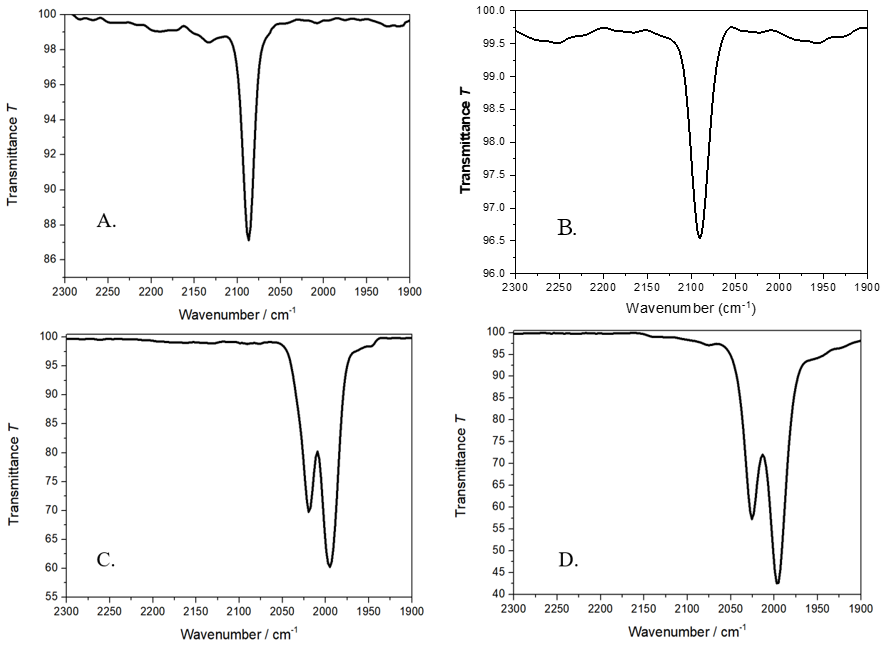

Figure S48. Solution state FTIR (THF) of copper(I) carbonyl adducts. (A) **L**$_1$CuCO, (B). **L**$_2$CuCO, (C) **L**$_3$CuCO, (D) **L**$_4$CuCO.

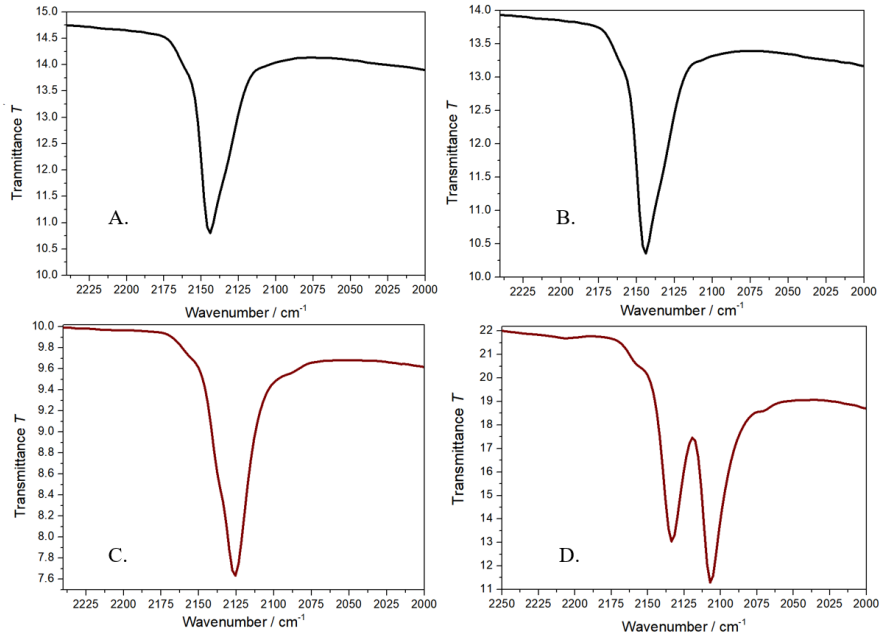

Figure S49. Solid state FTIR (KBr) of copper(I) isocyanide adducts. (A) **L**$_1$CuCNR, (B) **L**$_2$CuCNR, (C) **L**$_3$CuCNR, (D) **L**$_4$CuCNR.

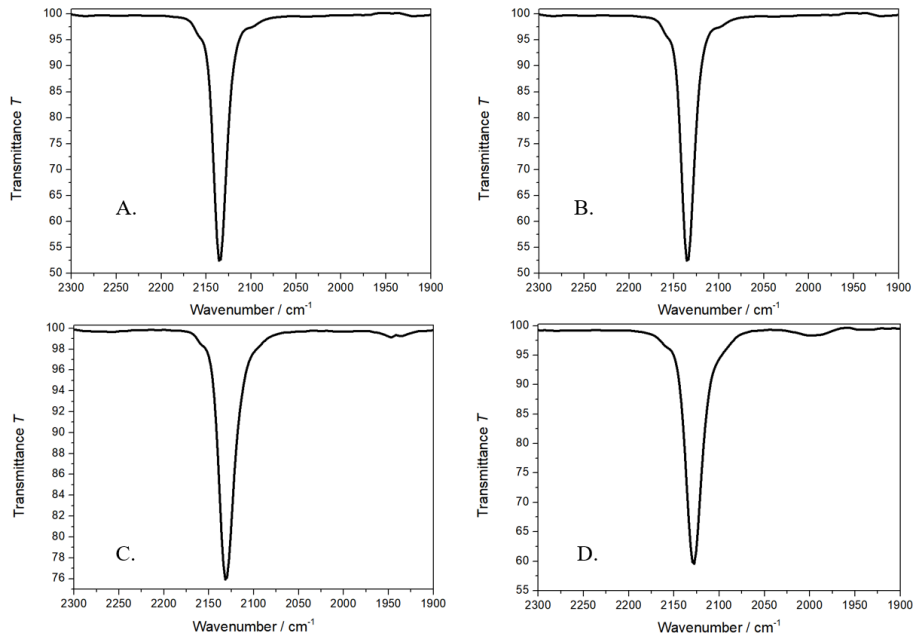

Figure S50. Solution state FTIR (THF) of copper(I) isocyanide adducts. (A) **L**$_1$CuCNR, (B) **L**$_2$CuCNR, (C) **L**$_3$CuCNR, D. **L**$_4$CuCNR

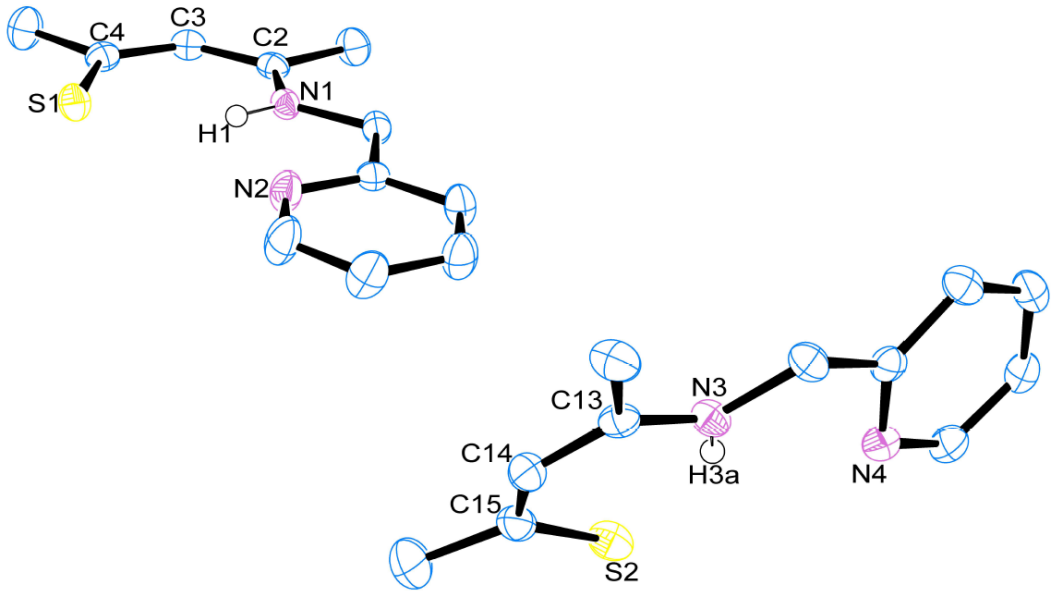

Figure S51. ORTEP X-ray structure of H**L**$_3$ at the 50% probability level. Hydrogen atoms are not shown for clarity except H_1 and H_{3a} group.

(A)

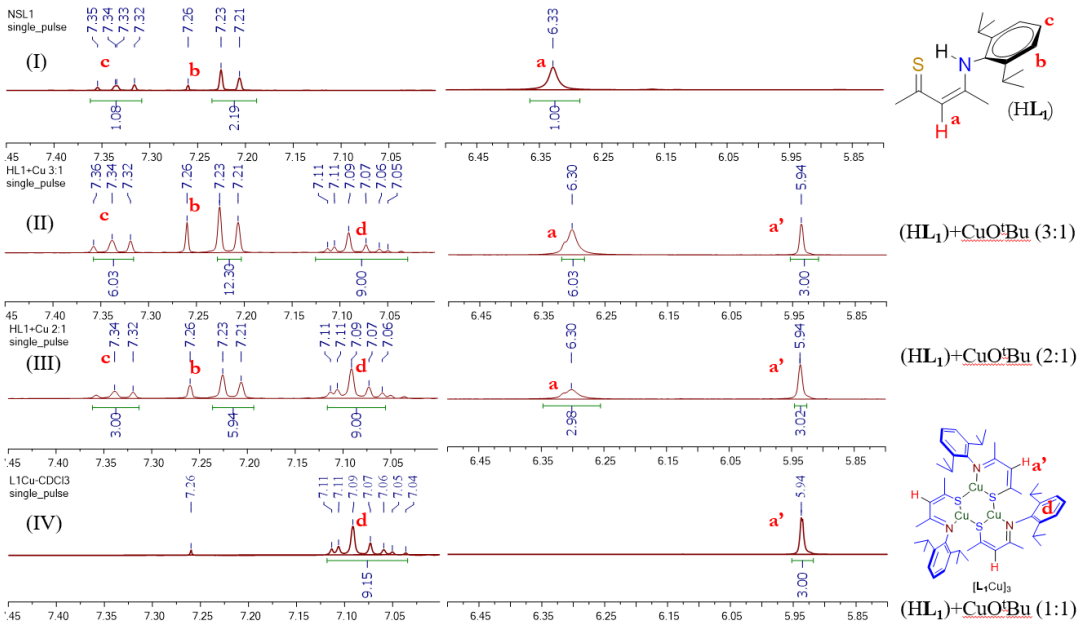
NSL1
single_pulse
(I)
HL1+Cu 3:1
single_pulse
(II)
HL1+Cu 2:1
single_pulse
(III)
L1Cu-CDCl3
single_pulse
(IV)
(HL1)
(HL1)+CuOtBu (3:1)
(HL1)+CuOtBu (2:1)
[L1Cu]3
(HL1)+CuOtBu (1:1)

(B)

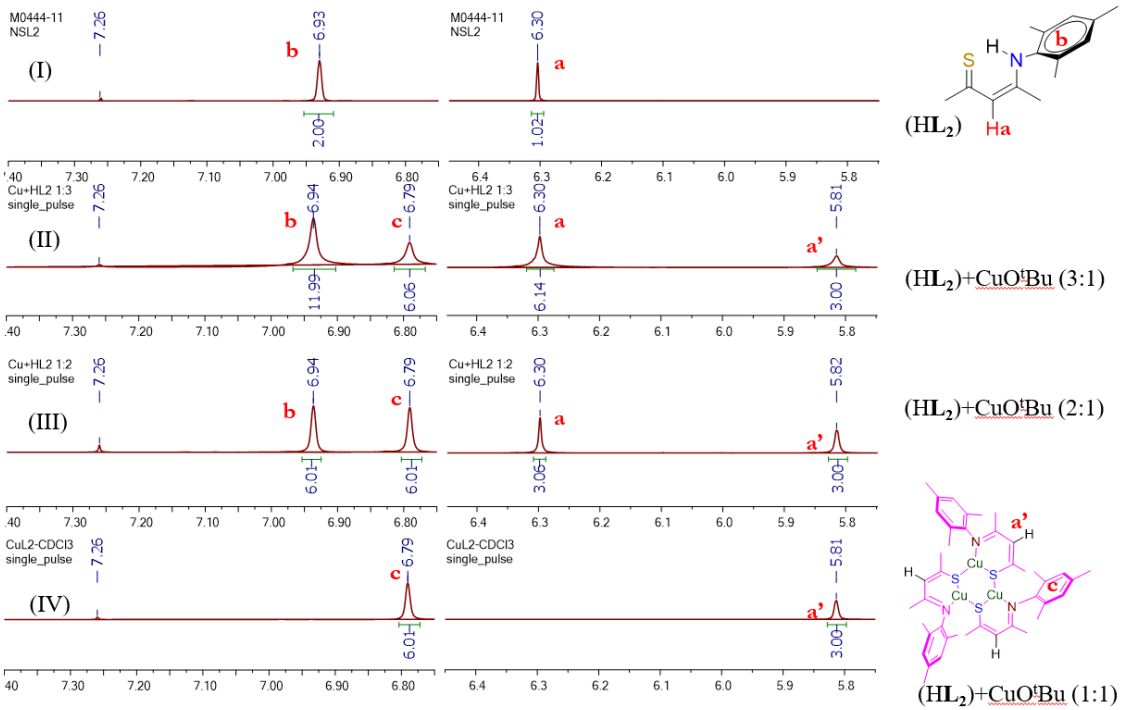
M0444-11
NSL2
(I)
Cu+HL2 1:3
single_pulse
(II)
Cu+HL2 1:2
single_pulse
(III)
CuL2-CDCl3
single_pulse
(IV)
(HL2)
(HL2)+CuOtBu (3:1)
(HL2)+CuOtBu (2:1)
(HL2)+CuOtBu (1:1)

(C)

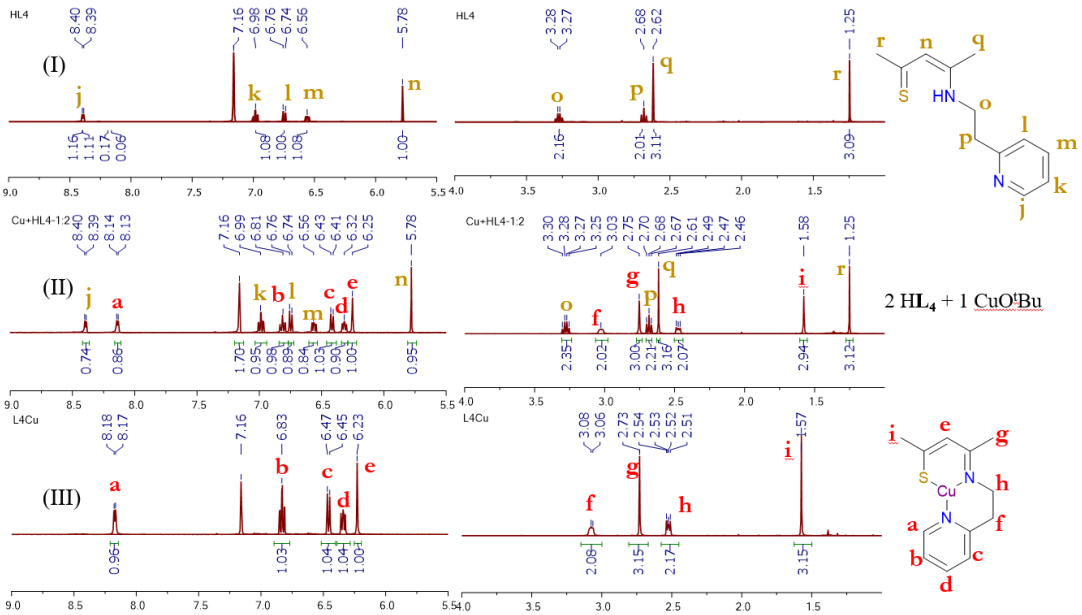

Figure S52. Stiochiometry-dependent NMR titration was performed at different concentrations in $CDCl_3$. The ^1H NMR spectra were recorded for the following samples: (A) Expanded regions 7.00 to 7.45 ppm and 5.80 to 6.50 ppm for I, only H**L**$_1$; II, CuO^tBu + H**L**$_1$ in 1:3 equivalents; III, CuO^tBu + H**L**$_1$ in 1:2 equivalents; IV, only [**L**$_1$Cu]$_3$. (B) Expanded regions 6.75 to 7.40 ppm and 5.80 to 6.50 ppm for I, only H**L**$_2$; II, CuO^tBu + H**L**$_2$ in 1:3 equivalents; III, CuO^tBu + H**L**$_2$ in 1:2 equivalents; IV, only [**L**$_2$Cu]$_3$. (C) Expanded regions 9.00 to 5.00 ppm and 4.00 to 1.00 ppm for I, only H**L**$_4$; II, CuO^tBu + H**L**$_4$ in 1:2 equivalents; III, only **L**$_4$Cu.

(A)

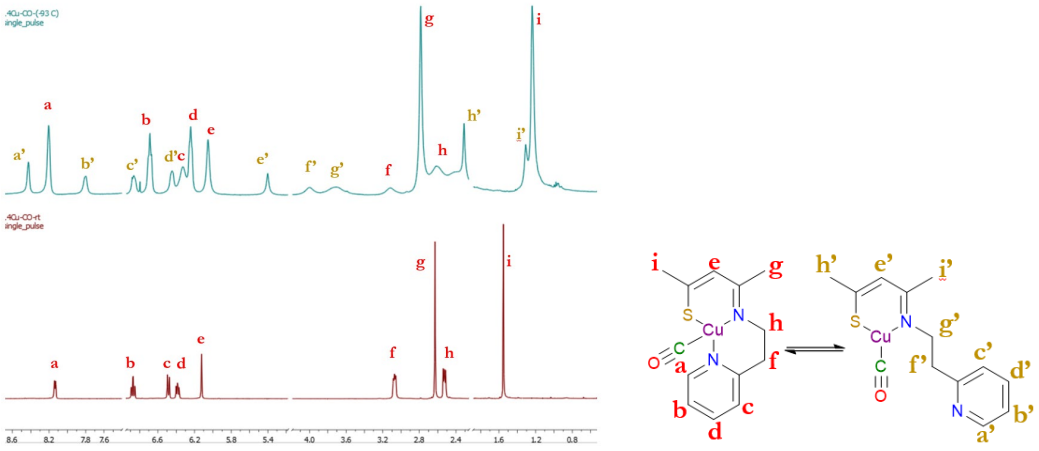

(B)

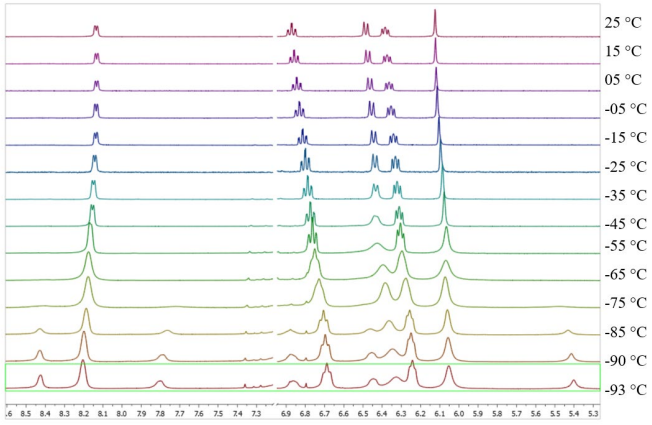

(C)

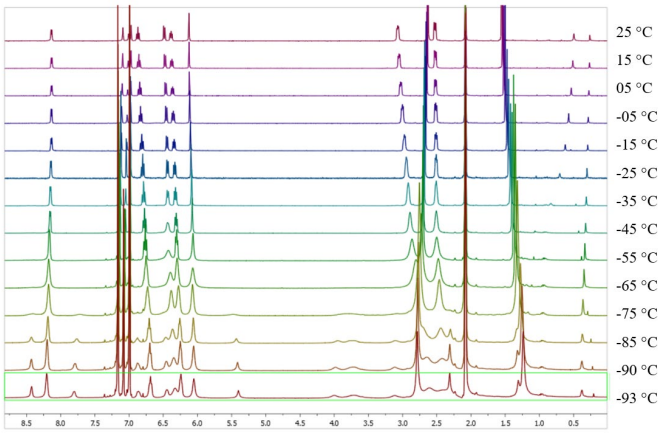

Figure S53. (A) The variable temperature ^{1}H NMR spectra of **L**$_{4}$CuCO in toluene-d8 were obtained at -93 °C and 25 °C, with an expanded region of 0.5 to 4.2 ppm and 5.2 to 8.6 ppm. (B) The expanded region of 5.2 to 8.6 ppm was studied using variable temperature ^{1}H NMR

spectroscopy for **L**$_4$CuCO. (C) The full ^{1}H NMR spectrum of **L**$_4$CuCO, along with the toluene-d8 peaks, was recorded.

Note: Toluene-d8 peaks were avoided for clarity for both A and B at 2.0 to 2.2 ppm and 7.0 to 7.2 ppm.

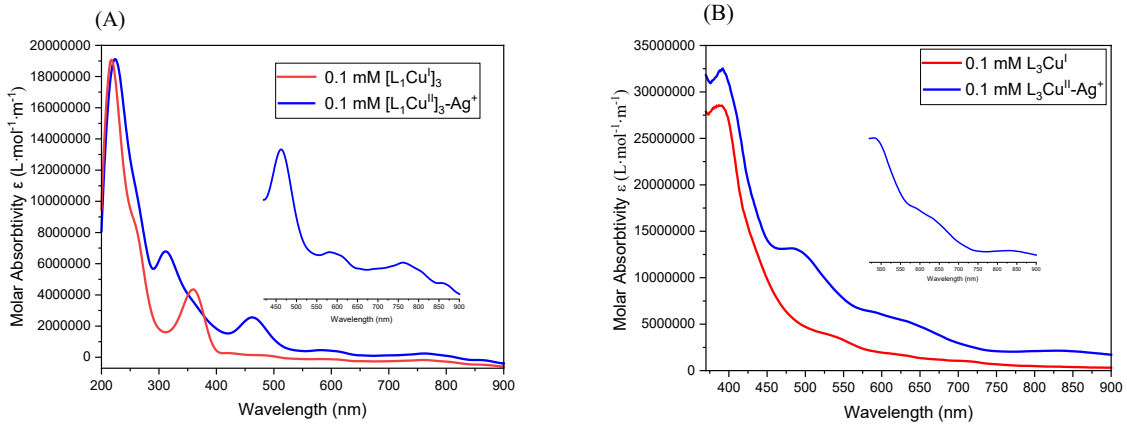

Figure S54. UV absorbance change for 0.1 mM (A) [**L**$_1$Cu]$_3$ and (B) **L**$_3$Cu complexes before and after treatment with Ag^+ in acetonitrile at room temperature. The insets show the increases in the d–d transition band intensities.

Note: We performed stoichiometry-dependent UV titration experiments in acetonitrile to observe the mixed [**L**$_1$Cu]$_3$ and its copper (II) products as shown in the scheme below. Unreacted [**L**$_1$Cu]$_3$ complexes could be extracted by ether to the expected yield.

(A) 1 [**L**$_1$Cu]$_3$ + 0.66 $AgClO_4$ $\xrightarrow{MeCN}$ 0.33 [**L**$_1$Cu]$_3$ + 0.66 [**L**$_1$Cu^{II}(NCMe)$_n$]ClO_4 + 0.66 Ag_0
(expected products)

(B) 1 **L**$_3$Cu + 1 $AgClO_4$ $\xrightarrow{MeCN}$ [**L**$_3$Cu^{II}(NCMe)$_n$]ClO_4 + Ag_0
(expected products)

Scheme S1. Stoichiometry-dependent oxidation control experiments. (A) Stoichiometry dependent titration of [**L**$_1$Cu]$_3$ with $AgClO_4$ in MeCN at room temperature. (B) Treatment of **L**$_3$Cu by $AgClO_4$ in MeCN at room temperature.

Table S1. Selected bond distances (Å) and bond angles (deg) for **L1**Cu(2,4,6-$CNC_6H_2Me_3$), **L2**Cu(2,4,6-$CNC_6H_2Me_3$), and **L4**Cu(2,4,6-$CNC_6H_2Me_3$).

	L1Cu(2,4,6-$CNC_6H_2Me_3$)	**L2**Cu(2,4,6-$CNC_6H_2Me_3$)[b]	**L4**Cu(2,4,6-$CNC_6H_2Me_3$)	
			Molecule A	Molecule B
Cu−N(amide(aryl))	1.973(16)	1.970(4)		
Cu−N(amide(alkyl))			2.046(19)	1.952(2)
Cu−N(Py)			2.110(2)	
Cu−S	2.174(5)	2.175(13)	2.268(7)	2.172(7)
C−C(NCCCS backbone)	1.436(3)	1.433(7)	1.443(3)	1.438(4)
	1.364(3)	1.358(7)	1.359(4)	1.362(4)
C−N	1.302(7)	1.308(6)	1.303(3)	1.477(3)
C−S	1.719(2)	1.730(5)	1.725(3)	1.721(3)
Cu−C(isocyanide)	1.848(2)	1.844(5)	1.867(3)	1.834(3)
C≡N(isocyanide)	1.154(3)	1.157(6)	1.164(3)	1.161(3)
N(amide(alkyl))−Cu−N(Py)			90.20(8)	
N(amide(aryl))−Cu−S	103.49(5)	102.79(12)		
N(amide(alkyl))−Cu−S			99.19(5)	104.48(6)
C(isocyanide)−Cu−S	136.33(6)	136.35(15)	118.29(7)	130.81(8)
C(isocyanide)−Cu−N(amide(aryl))	120.19(8)	120.44(19)	109.58(9)	124.60(10)
∠NCCCS(aryl)[a]	86.50	88.79		

[a] Dihedral angle between NCCCS plane and the *N*-aryl ring. [b] There are three independent molecules of **L2**Cu(2,4,6-$CNC_6H_2Me_3$) in the unit cell, only one molecule data shown here. For complete information refer supporting information Figure S47 and Table S3.

Table S2. Selected Bond distances (Å) and Bond Angles (deg) for **L1**Cu(PPh3), **L2**Cu(PPh3), and **L4**Cu(PPh3).

	L1Cu(PPh3)	**L2**Cu(PPh3)[b]	**L4**Cu(PPh3)
Cu−N(amide(aryl))	1.956(3)	1.941(5)	
Cu−N(amide(alkyl))			2.049(17)
Cu−N(Py)			2.069(17)
Cu−S	2.204(9)	2.188(19)	2.256(6)
Cu−P	2.195(10)	2.182(19)	2.210(6)
C−C(NCCCS backbone)	1.431(5)	1.441(9)	1.448(3)
	1.363(5)	1.351(9)	1.365(3)
C−N	1.315(5)	1.312(8)	1.296(3)
C−S	1.721(4)	1.726(7)	1.720(2)
P−Cu−S	116.88(4)	122.41(7)	114.15(2)
N(amide(aryl))−Cu−P	139.42(9)	133.96(15)	
N(amide(alkyl))−Cu−P			115.54(5)
N(amide(aryl))−Cu−S	103.68(9)	103.53(15)	
N(amide(alkyl)−Cu−S			100.28(5)
N(amide(alkyl))−Cu−N(Py)			90.93(7)
∠NCCCS(aryl)[a]	82.93	83.49	

[a] Dihedral angle between NCCCS plane and the *N*-aryl ring. [b] There are two independent molecules of **L2**Cu(PPh3) in the unit cell, only one molecule data shown here. For complete information see figures S46, S48 and Table S3.

Table S3. Selected bond lengths (Å) and bond angles (°) for copper(I) adducts, **L**$_2$Cu(2,4,6-$CNC_6H_2Me_3$) and **L**$_2$CuPPh$_3$.

	L$_2$Cu(2,4,6-$CNC_6H_2Me_3$)[b]	**L**$_2$Cu(2,4,6-$CNC_6H_2Me_3$)[b]	**L**$_2$Cu(2,4,6-$CNC_6H_2Me_3$)[b]	**L**$_2$CuPPh$_3$[c]	**L**$_2$CuPPh$_3$[c]
Cu−N(amide(aryl))	1.970(4)	1.977(4)	1.950(4)	1.941(5)	1.937(5)
Cu−S	2.175(13)	2.161(13)	2.175(15)	2.188(19)	2.187(2)
Cu−P				2.182(19)	2.183(19)
C−C(NCCCS backbone)	1.433(7) 1.358(7)	1.440(7) 1.361(6)	1.441(7) 1.360(7)	1.441(9) 1.351(9)	1.433(9) 1.353(9)
C−N	1.308(6)	1.297(6)	1.307(6)	1.312(8)	1.305(8)
C−S	1.730(5)	1.729(5)	1.706(5)	1.726(7)	1.723(7)
Cu−C(isocyanide)	1.844(5)	1.837(5)	1.835(5)		
C≡N(isocyanide)	1.157(6)	1.161(6)	1.155(6)		
P−Cu−S				122.41(7)	122.08(8)
N(amide(aryl))−Cu−P				133.96(15)	134.67(17)
N(amide(aryl))−Cu−S	102.79(11)	103.87(11)	104.89(12)	103.53(15)	103.07(17)
C(isocyanide)−Cu−S	136.35(15)	142.51(16)	132.79(17)		
C(isocyanide)−Cu−N(amide (aryl))	120.44(19)	113.53(19)	122.0(2)		
∠NCCCS(aryl)[a]	88.79	88.54	89.92	83.49	85.72

[a]Dihedral angle between N-aryl ring and NCCCS plane. [b]There are three independent crystal structures of **L**$_2$Cu(2,4,6-$CNC_6H_2Me_3$) see figure S47 similar to each other in same unit cell. [c]There are two independent crystal structures of **L**$_2$Cu(PPh_3) similar to each other in same unit cell.

Table S4. Crystallographic data for synthesized ligands H**L**$_1$, H**L**$_2$, H**L**$_3$, H**L**$_4$ and copper(I) complexes [**L**$_1$Cu]$_3$, **L**$_3$Cu

	H**L**$_1$[a]	H**L**$_2$	H**L**$_3$	H**L**$_4$	[**L**$_1$Cu]$_3$	**L**$_3$Cu
CCDC Number	2177690	2177691	2177692	2177693	2177697	2177698
Empirical formula	C_{17} H_{24} N S	C_{14} H_{19} N S	C_{22} H_{28} N_4 S_2	C_{12} H_{16} N_2 S	C_{50} H_{70} Cu_3 N_3 S_3	C_{11} H_{13} Cu N_2 S
Formula weight	274.43	233.36	412.60	220.33	999.89	268.83
T° K	113(2)	113(2)	113(2)	113(2)	113(2)	113(2)
Crystal size mm^3	0.3 x 0.25 x 0.2	0.25 x 0.2 x 0.2	0.25 x 0.2 x 0.2	0.25 x 0.2 x 0.2	0.2 x 0.15 x 0.1	0.25 x 0.2 x 0.2
Crystal system	Monoclinic	Monoclinic	Triclinic	Triclinic	Orthorhombic	Triclinic
Space group	$P2_1/c$	$P2_1/c$	P-1	P-1	$P2_12_12_1$	P-1
a(Å)	11.8498(4)	8.1962(3)	6.8410(2)	7.0013(5)	15.3411(3)	7.5980(3)
b(Å)	8.9288(4)	8.8474(2)	9.3645(3)	7.2355(5)	16.6809(3)	7.7676(3)
c(Å)	15.6583(6)	18.7562(5)	18.5881(4)	12.2312(9)	19.9753(4)	10.3763(4)
α(deg)	90°	90°	93.715(2)°	105.091(6)°	90°	102.817(3)°
β(deg)	99.025(3)°	100.089(3)°	99.741(2)°	93.555(6)°	90°	98.971(3)°
γ(deg)	90°	90°	107.792(3)°	92.253(6)°	90°	107.163(4)°
V (Å^3)	1636.21(11)	1339.08(7)	1108.86(6)	596.10(8)	5111.75(17)	554.20(4)
Z	4	4	2	2	4	2
D_{calcd} (g cm^{-3})	1.118	1.158	1.236	1.228	1.299	1.611
μ(mm^{-1})	0.186	0.216	0.255	0.241	1.394	2.124
Reflns mcasd/indep	13693/2888	19261/2818	15514/4610	6999/ 2447	33473/10353	6328/2274
Data/restrains/params	2888/102/182	2818 / 0 / 150	4610 / 0 / 257	2447 / 0 / 138	10353 / 306 / 561	2274 / 0 / 138
GOF	1.065	1.072	1.071	1.073	1.034	1.144
R_{int}	0.0297	0.0242	0.0295	0.0407	0.0729	0.0574
R_I[I>2σ] (all data)	0.0367 (0.0914)	0.0328(0.0834)	0.0355 (0.0812)	0.0444 (0.1185)	0.0570 (0.1258)	0.0355 (0.0841)
R_w[I>2σ] (all data)	0.0446 (0.0952)	0.0387(0.0860)	0.0454 (0.0850)	0.0547 (0.1232)	0.0667 (0.1298)	0.0417 (0.0863)
Max. peak/hole (e$^-$/ Å^3)	0.18/ -0.21	0.23 / -0.21	0.29 / -0.21	0.423 / -0.320	0.820 / -0.642	0.511 / -0.744

[a]The N-H hydrogen of H**L**$_1$ also could be confirmed by the NMR characterizations in comparison with H**L**$_2$ analogue.

Table S5. Crystallographic data for synthesized copper(I) phosphine and isocyanide adducts

	L$_1$Cu(2,4,6-$CNC_6H_2Me_3$)	**L**$_2$Cu(2,4,6-$CNC_6H_2Me_3$)	**L**$_4$Cu(2,4,6-$CNC_6H_2Me_3$)	**L**$_1$Cu(PPh_3)	**L**$_2$Cu(PPh_3)	**L**$_4$Cu(PPh_3)
CCDC Number	2260182	2177695	2177696	2177687	2177688	2177689
Empirical formula	$C_{27}H_{35}CuN_2S$	$C_{72}H_{87}Cu_3N_6S_3$	$C_{44}H_{52}Cu_2N_6S_2$	$C_{35}H_{39}CuNPS$	$C_{64}H_{66}Cu_2N_2P_2S_2$	$C_{30}H_{30}CuN_2PS$
Formula weight	483.17	441.09	856.1	600.24	1116.32	545.13
T° K	113(2)	113(2)	113(2)	113(2)	113(2)	113(2)
Crystal size mm^3	0.3 x 0.2 x 0.2	0.2 × 0.15 × 0.1	0.38 × 0.25 × 0.25	0.25 × 0.15 × 0.1	0.2 × 0.15 × 0.1	0.3 × 0.2 × 0.2
Crystal system	Tetragonal	Monoclinic	Triclinic	Monoclinic	Monoclinic	Monoclinic
Space group	P-42$_1$c	$P2_1/c$	P-1	Pn	$P2_1/c$	$P2_1/c$
a(Å)	10.195(3)	8.3921(2)	8.4434(3)	8.7209(2)	34.0853(6)	10.0287(2)
b(Å)	11.398(3)	72.7477(11)	13.9072(4)	11.5302(2)	10.8570(2)	9.2600(2)
c(Å)	13.1968(3)	11.9258(3)	19.3518(6)	15.5452(3)	15.8802(4)	28.7420(6)
α(deg)	103.579(2)°	90°	99.445(2)°	90°	90°	90°
β(deg)	103.829(2)°	109.714(3)°	100.502(3)°	97.780(2)	102.842(2)°	96.315(2)°
γ(deg)	111.271(2)°	90°	105.746(3)°	90°	90°	90°
V ($Å^3$)	1297.18(7)	6854.0(3)	2094.97(12)	1548.74(5)	5729.7(2)	2652.95(10)
Z	2	12	4	2	4	4
D_{calcd} (g cm^{-3})	1.237	1.282	1.357	1.287	1.294	1.365
μ(mm^{-1})	0.938	1.058	1.153	0.848	0.912	0.984
Reflns mcasd/indep	37815/4553	63787/13864	43908/7357	25463/4673	48453/10040	21461/5531
Data/restrains/params	4553 / 0 / 289	13864/0/781	7357/0/497	4673/32/359	10040/0/660	5531/0/318
GOF	1.089	1.238	1.104	1.094	1.157	1.045
R_{int}	0.0576	0.0508	0.0295	0.0343	0.0828	0.0341
R_1[I>2σ] (all data)	0.0331 (0.0838)	0.0712 (0.1330)	0.0378 (0.1022)	0.0437, (0.1118)	0.0873 (0.1782)	0.0351 (0.0782)
R_w[I>2σ] (all data)	0.0385 (0.0858)	0.0941 (0.1388)	0.0460 (0.1068)	0.0463, (0.1124)	0.1121 (0.1873)	0.0469 (0.0818)
Max. peak/hole (e^-/ $Å^3$)	0.41/ -0.36	0.58/-0.71	0.73/ -0.46	0.33/-0.68	1.18/-0.75	0.46/-0.43

Table S6. Selected bond lengths (Å) and bond angles (°) for H**L**$_3$

	H**L**$_3$	
	Molecule I	Molecule II
C−C$_{(NCCCS\ backbone)}$	1.409(2), 1.381(2)	1.405(2), 1.380(2)
C−N$_{(NCCCS\ backbone)}$	1.317(18)	1.317(19)
C−S	1.698(16)	1.6959(17)
N−H	0.860	0.860

Table S7. CV data for [**L**$_1$Cu]$_3$, [**L**$_2$Cu]$_3$, **L**$_3$Cu, and **L**$_4$Cu complexes in MeCN solutions

Complex	E_a	E_c	i_{pa} / i_{pc}	$E_{1/2}$ (V)	ΔE(V)[c]
[**L**$_1$Cu]$_3$	-0.153	-	-	-	-
[**L**$_2$Cu]$_3$	-0.011	-	-	-	-
L$_3$Cu	-0.562	-0.692	0.93	-0.627	0.130[b]
L$_4$Cu	-0.286	-0.440	1.20	-0.363	0.154[b]

[a]All values reported vs NHE, by adding 0.64V to the value measured vs the ferrocene/ferrocenium couple in CH_3CN with Bu_4NPF_6 as electrolyte and potentials (in V vs. $Fc^{+/0}$) were measured at a glassy carbon electrode at a scan rate of 0.01Vs^{-1}.
b. Quasi-reversible.
c. $\Delta E = E_c - E_a$.

Table S8. Kinetic data and equilibrium constants of carbonylation and decarbonylation for β-thioketiminato copper(I) complexes.

$$[\mathbf{L}Cu^{I}] + [CO] \underset{N_2,\ k_{-CO}}{\overset{k_{CO}}{\rightleftharpoons}} [\mathbf{L}Cu^{I}\text{-}CO] \qquad \text{(S1)}$$

$$K_{CO} = \frac{k_{CO}}{k_{-CO}} \qquad \text{(S2)}$$

The equilibrium constants and the binding constants for carbonylation and decarbonylation experiments were calculated using the above equations (S1) and (S2).

Complex	Wavenumber (cm^{-1})	k_{CO}, M^{-1} s^{-1}	k_{-CO}, s^{-1}	K_{CO}, M^{-1}
[**L**$_1$Cu]$_3$	2085	4.77x10^{-4}(±0.17)	1.45x10^{-3}(±0.09)	0.32(±0.06)
[**L**$_2$Cu]$_3$	2085	1.09x10^{-3}(±0.04)	3.22x10^{-3}(±0.09)	0.33(±0.15)
L$_3$Cu	1995	5.91x10^{-3}(±0.05)	2.14x10^{-4}(±0.18)	27.61(±0.12)
	2019	4.57x10^{-3}(±0.26)	2.25x10^{-4} (±0.20)	20.31(±0.26)
L$_4$Cu	1995	8.91x10^{-3}(±0.67)	3.35x10^{-4}(±0.07)	26.53(±0.33)
	2020	5.35x10^{-3}(±0.59)	3.26x10^{-4}(±0.10)	16.40(±0.56)